

4 **Impact of jet production data on the next-to-next-to-leading order**
5 **determination of HERAPDF2.0 parton distributions**

6 **Paper Draft v1.0 – August 16, 2021**

7 Author list

8 **Abstract**

9 The HERAPDF2.0 [ensemble](#) of parton distribution functions (PDFs) was introduced in
10 2015. [Presented is the final stage, a next-to-next-to-leading order analysis of the HERA](#)
11 [data on inclusive deep inelastic \$ep\$ scattering together with jet data as published by H1](#)
12 [and ZEUS. A pQCD fit to the data with free \$\alpha_s\(M_Z^2\)\$ and free PDFs was used to determine](#)
13 [\$\alpha_s\(M_Z^2\)\$ with the result \$\alpha_s\(M_Z^2\) = 0.1156 \pm 0.0011\$ \(exp\) \$^{+0.0001}_{-0.0002}\$ \(model + parameterisation\) \$\pm\$](#)
14 [0.0029 \(scale\). The HERAPDF2.0Jets NNLO sets of parton density functions from fits with](#)
15 [fixed \$\alpha_s\(M_Z^2\) = 0.1155\$ and \$\alpha_s\(M_Z^2\) = 0.118\$, the value used for the published HERA-](#)
16 [PDF2.0 NNLO analysis based on inclusive data only, are presented and compared. The](#)
17 [PDFs of HERAPDF2.0Jets NNLO for fixed \$\alpha_s\(M_Z^2\) = 0.118\$ are also compared to the PDFs](#)
18 [of HERAPDF2.0 NNLO. The similarity of the PDFs demonstrates the consistency of inclu-](#)
19 [sive and jet-production cross-section data. Predictions based on HERAPDF2.0Jets NNLO](#)
20 [agree very well with the jet-production data used in the fits.](#)

21 *To be submitted to EPJC*

1 Introduction

Data from deep inelastic scattering (DIS) of electrons¹ on protons, ep , at centre-of-mass energies of up to $\sqrt{s} \approx 320$ GeV at HERA have been central to the exploration of proton structure and quark–gluon dynamics as described by perturbative Quantum Chromo Dynamics (pQCD) [1].

The combination of H1 and ZEUS data on inclusive ep scattering and the subsequent pQCD analysis, introducing the ensemble of parton density functions (PDFs) known as HERAPDF2.0, were milestones for the exploitation [2] of the HERA data. The HERAPDF analyses are based on pQCD fits to the HERA DIS data in the DGLAP [3–7] formalism in the $\overline{\text{MS}}$ scheme [8].

The sets of PDFs presented in this work complete the HERAPDF2.0 ensemble [2] of PDFs. They were determined with an NNLO analysis of HERA inclusive and selected jet-production data as published separately by the H1 and ZEUS collaborations [9–14]. An analysis of jet data at NNLO was not possible at the time of the introduction of the HERAPDF2.0 ensemble. It became possible when predictions of jet cross-section at NNLO [15–23] for ep became available.

The strategy of the analysis follows the strategy of the original and verified pQCD [2] analysis at NLO. As the value of the strong coupling constant, $\alpha_s(M_Z^2)$, cannot be separated from the PDFs resulting from any pQCD fit, a suitable value of $\alpha_s(M_Z^2)$ has to be determined first by fitting the PDFs and $\alpha_s(M_Z^2)$ simultaneously. This avoids biases on $\alpha_s(M_Z^2)$ as would be introduced by fitting $\alpha_s(M_Z^2)$ with fixed PDFs [24]. In a second step, the PDFs are refined by a fit with $\alpha_s(M_Z^2)$ fixed to the optimised value.

The calculation of jet cross-sections at NNLO constructs jets starting from massless partons. The inclusive data, on the other hand, are treated within the RTOPT [25–27] Variable Flavour Number Scheme (VFNS), which requires values of the parameters for the charm and bottom masses, M_c and M_b , as input. These parameters were optimised using cross sections for charm and bottom production, which were published as combined data by the H1 and ZEUS collaborations together with a pQCD analysis [28]. An inclusion of the heavy-quark data in the pQCD fit including jets is considered inappropriate due to the different treatment of heavy-quark masses for the predictions on inclusive and jet data.

The results presented here are based entirely on HERA data, i.e. inclusive and jet-production data. The HERA inclusive data represent a single, highly consistent data set. Furthermore, the jet data have been found to be very consistent with the inclusive data at NLO [2]; the analysis presented here also tests consistency at NNLO. In addition, DIS is the only process for which the factorisation theorem is fully established. It is only a standard assumption that it is also valid for hadron-hadron interaction processes. However, even if this assumption is valid, PDF fits to LHC data would be biased by any physics Beyond the Standard Model (BSM) whose effects have so far escaped detection, thereby reducing the sensitivity of searches for BSM due to biased background predictions. Thus, the HERAPDF2.0 ensemble of PDFs provides a benchmark to which PDFs including data from LHC colliders may be compared. This could reveal BSM effects or the need for an extension of the QCD analyses for some processes.

¹From here on, the word “electron” refers to both electrons and positrons, unless otherwise stated.

2 Data

Data taken by the H1 and ZEUS collaborations from 1993 to 2007 were combined to form a coherent set of inclusive HERA ep DIS cross sections [2], which was used as input to the determinations of all previous members of the HERAPDF2.0 ensemble. The HERAPDF2.0Jets analysis at NLO, in addition, used selected data [9–12,14] on inclusive jet and dijet production from H1 and ZEUS, which were again used for the present analysis at NNLO. In addition, new data [13], published by the H1 collaboration on jet production in lower Q^2 events, where Q^2 is the four-momentum-transfer squared, together with six new high- Q^2 points at low p_T , where p_T is the transverse energy of the jet, which were published by H1 in the same publication to complete the previously published high- Q^2 data set [14], were added as input to the NNLO analysis. A summary on the data of jet production used is provided in Table 1. For all data sets, the jets were identified with the k_T algorithm with the R parameter set to one.

The new treatment of inclusive jet and dijet production at NNLO was, however, only applicable to a slightly reduced phase space compared to HERAPDF2.0Jets NLO. All data points with $\mu = \sqrt{\langle p_T^2 \rangle + Q^2} \leq 10.0 \text{ GeV}$ had to be excluded in order to ensure the convergence of the perturbative series and to limit the NNLO scale uncertainties of the theoretical predictions to below 10 % compared to below 24 % at NLO. This requirement on μ also ensured that μ was larger than the b-quark mass, which is necessary because the jets are assumed to be built from massless partons in the calculation of the NNLO predictions. In addition, for each Q^2 bin, the six data points with the lowest $\langle p_T \rangle$ had to be excluded from the ZEUS dijet data set because the available NNLO predictions for these points were judged to be incomplete considering the kinematic cuts². The resulting reduction of data points is detailed in Table 1. In addition, the trijet data [14] which were used as input to HERAPDF2.0Jets NLO had to be excluded as no NNLO treatment was available.

The inclusive charm data [29], which were included in the analysis at NLO [2] were not explicitly used in the PDF fits of the analysis presented here, since complete NNLO predictions were not available. Heavy quark data [28] were only used to optimise the mass parameter values for charm, M_c , and beauty, M_b , which are needed as input to the adopted RTOPT [27] NNLO approach to the fitting of the inclusive data.

3 QCD Analysis

The analysis presented here was done along the same lines as all previous HERAPDF2.0 analyses [2]. Only cross sections for Q^2 starting at $Q_{min}^2 = 3.5 \text{ GeV}^2$ were used in the analysis. The χ^2 definition was taken from equation 32 of the previous paper [2]. The value of the starting scale for the evolution was taken as $\mu_{f0}^2 = 1.9 \text{ GeV}^2$. The parameterisation and choice of free parameters also followed the prescription for the HERAPDF2.0Jets NLO fit, see Section 3.1 below.

All fits were performed using the programme QCDNUM [30] within the xFitter, formerly HERAFitter, framework [31] and were cross-checked with an independent programme, which

²Due to the kinematic cuts used in selecting the dijet data, the LO prediction for the cross sections is zero. Thus, the NNLO term is only the second non-zero term.

was already used as a second programme in the HERAPDF2.0 analysis. The results obtained using the two programmes, as previously for all HERAPDF2.0 fits [2], were in excellent agreement, i.e. well within fit uncertainties. All numbers presented here were obtained using xFitter.

The light-quark coefficient functions were calculated in QCDNUM. The heavy-quark coefficient functions were calculated in the general-mass variable-flavour-number scheme RTOPT [25], with recent modifications [26,27].

The analysis presented here became possible due to the newly available treatment of jet production at NNLO, using the zero-mass scheme. This is expected to be a reasonable approximation when the relevant QCD scales are significantly above the charm- and beauty-quark masses. The jet data were included in the fits at full NNLO using predictions for the jet cross sections calculated using NNLOJET [15–17], which was interfaced to the fast interpolation grid codes, fastNLO [18–20] and APPLgrid [21,22] using the APPLfast framework [23], in order to achieve the required speed for the convolutions needed in an iterative PDF fit. The NNLO jet predictions were provided in the massless scheme and were corrected for hadronisation and Z^0 exchange before they were used in the fits. A running electro magnetic α as implemented in the 2012 version of the programme EPRC [32] was used in the treatment of the jet cross sections. The predictions were provided with fully correlated uncertainties, which were taken into account in all fits.

The choice of scales for the jet data had to be adjusted for the NNLO analysis. At NLO, the factorisation scale was chosen as for the inclusive data, i.e. $\mu_f^2 = Q^2$, while the renormalisation scale was linked to the transverse momenta, p_T , of the jets as $\mu_r^2 = (Q^2 + p_T^2)/2$. For the NNLO analysis, $\mu_f^2 = \mu_r^2 = Q^2 + p_T^2$ was used. This resulted in an improved χ^2 for the fits. Scale variations were also considered and are discussed in Sections 4.1 and 4.2.

3.1 Choice of parameterisation and model parameters

The PDFs were parameterised as a function of x at the input scale by the generic form

$$xf(x) = Ax^B(1-x)^C(1+Dx+Ex^2). \quad (1)$$

The PDF of the gluon was an exception, for which an additional term of the form $A'_g x^{B'_g}(1-x)^{C'_g}$ was subtracted³. This choice of parameterisation follows the original concept of HERAPDF2.0, for which all details were previously published [2]. The parameterisation is an effective way to store the information derived from many data points in a limited set of numbers.

The parameterised PDFs are the gluon distribution xg , the valence-quark distributions xu_v , xd_v , and the u -type and d -type anti-quark distributions $x\bar{U}$, $x\bar{D}$, where $x\bar{U} = x\bar{u}$ and $x\bar{D} = x\bar{d} + x\bar{s}$ at the chosen starting scale. The parameterisation for the central fit was determined by initially fixing the D , E and A'_g parameters to zero. This resulted in 10 free parameters. The extra parameters were introduced one at a time until the χ^2 of the fit could not be further improved [2,33]. This is also called the χ^2 saturation method. This resulted in a 14 parameter fit which satisfied the criteria that all PDFs and all predicted cross sections were positive throughout

³The parameter $C'_g = 25$ was fixed since the fit is not sensitive to this value, provided it is high enough ($C'_g > 15$) ensuring that the term does not contribute at large x .

the kinematic region probed by the data entering the fit. The suitability of the parameterisation was, thus, also verified for the selection of jet data.

The final parameterisation was

$$xg(x) = A_g x^{B_g} (1-x)^{C_g} - A'_g x^{B'_g} (1-x)^{C'_g}, \quad (2)$$

$$xu_v(x) = A_{u_v} x^{B_{u_v}} (1-x)^{C_{u_v}} (1 + E_{u_v} x^2), \quad (3)$$

$$xd_v(x) = A_{d_v} x^{B_{d_v}} (1-x)^{C_{d_v}}, \quad (4)$$

$$x\bar{U}(x) = A_{\bar{U}} x^{B_{\bar{U}}} (1-x)^{C_{\bar{U}}} (1 + D_{\bar{U}} x), \quad (5)$$

$$x\bar{D}(x) = A_{\bar{D}} x^{B_{\bar{D}}} (1-x)^{C_{\bar{D}}}. \quad (6)$$

The normalisation parameters, A_g, A_{u_v}, A_{d_v} , were constrained by the quark-number and momentum sum rules. The B parameters, $B_{\bar{U}}$ and $B_{\bar{D}}$, were set equal, $B_{\bar{U}} = B_{\bar{D}}$, such that there was a single B parameter for the sea distributions.

The strange-quark distribution was expressed as an x -independent fraction, f_s , of the d -type sea, $x\bar{s} = f_s x\bar{D}$ at Q_0^2 . The central value $f_s = 0.4$ was chosen to be a compromise between the determination of a suppressed strange sea from neutrino-induced di-muon production [34,35] and the determination of an unsuppressed strange sea from the ATLAS collaboration [36]. The further constraint $A_{\bar{U}} = A_{\bar{D}}(1-f_s)$, together with the requirement $B_{\bar{U}} = B_{\bar{D}}$, ensured that $x\bar{u} \rightarrow x\bar{d}$ as $x \rightarrow 0$.

3.2 Model and parameterisation uncertainties

Model and parameterisation uncertainties on the PDFs determined by a central fit were evaluated with fits with modified input assumptions. The central values of the model parameters and their variations are summarised in Table 2. The value of $\alpha_s(M_Z^2)$ is either fixed to the input value or free for the simultaneous fit of $\alpha_s(M_Z^2)$ and the PDFs.

The uncertainties on the PDFs obtained from variations of M_c, M_b, f_s, Q_{min}^2 were added in quadrature, separately for positive and negative uncertainties, and represent the model uncertainty.

The uncertainty obtained from the variation of μ_{f0}^2 was added to the parameterisation uncertainty. A variation of the number of terms in the polynomial $(1 + Dx + Ex^2)$ was considered for each of the parton distributions listed in Eqs. 2–6. For this, all 15-parameter fits which have one more non-zero free D or E parameter were considered as possible variants and the resulting PDFs compared to the PDF from the 14-parameter central fit. The only significant change in the PDFs was observed for the addition of a D_{u_v} parameter. The uncertainties on the central fits from the parameterisation variations were stored as an envelope representing the maximal deviation at each x value.

The total uncertainties on the PDFs were obtained by adding experimental, i.e. fit, model and parameterisation uncertainties in quadrature.

3.3 Optimisation of M_c and M_b

The RTOPT scheme used to calculate predictions for the inclusive data requires the charm- and beauty-mass parameters, M_c and M_b , as input. The optimal values of these parameter were reevaluated using new combined HERA data, which became available [28], superseding the previously published combination of charm data [29] and the data published separately by H1 and ZEUS on beauty production. The optimisation was done using the standard procedure [?] through fits to the inclusive HERA data together with the new combined heavy-flavour data with varying choices of the mass parameter values. The values resulting in the lowest χ^2 values of the fit were chosen for the jet analysis. This was done both at NLO to facilitate the pQCD analysis at NLO published previously [28] and at NNLO for the analysis presented here. The one standard-deviation uncertainties of the mass parameters were determined by fitting the χ^2 values with a quadratic function and finding the mass-parameter values corresponding to $\Delta\chi^2 = 1$ values.

At NNLO, the fits for the optimisation were performed using the fixed value of $\alpha_s = 0.1155$ ⁴; at NLO, $\alpha_s = 0.118$ was used. As a first iteration at NNLO (NLO), M_c was varied with fixed $M_b = 4.5$ GeV (4.5 GeV) and M_b was varied with fixed $M_c = 1.43$ GeV (1.47 GeV), i.e. the mass-parameter values used for HERAPDF2.0 NNLO (NLO) were used as fix-points. In every iteration, the mass-parameter values as obtained in the previous iteration were used as new fix-points. The iteration was ended once values stable to 0.1 % for M_c and M_b were observed. The final χ^2 scans at NNLO are shown in Figs. 1 a) and c) and at NLO Figs. 1 b) and d). The resulting values at NNLO are $M_c = 1.41 \pm 0.04$ GeV and $M_b = 4.20 \pm 0.10$ GeV, quite close to the values determined for HERAPDF2.0 NNLO, with slightly reduced uncertainties. The values at NLO are $M_c = 1.46 \pm 0.04$ GeV and $M_b = 4.30 \pm 0.10$ GeV. The minima in χ^2 for M_b demonstrate the power of the method. The minimum in χ^2 for the parameter M_c at NNLO is observed close to the technical limit of the fitting procedure.

The part of the model uncertainty concerning the heavy-flavour mass parameters would nominally have involved varying the value of M_c to the minimum and maximum of its one standard-deviation uncertainty. However, for M_c , the downward variation created a conflict with μ_{f0} , which has to be less than M_c in the RTOPT scheme, such that charm can be generated perturbatively. Thus, only an upward variation of M_c was considered and the resulting uncertainty on the PDFs was symmetrised. In addition, the condition $\mu_{f0} < M_c$ created a conflict with the variation of μ_{f0}^2 . The normal procedure would have included an upward variation of μ_{f0}^2 to 2.2 GeV² but μ_{f0} would have become larger than the upper end of the uncertainty interval of M_c ⁵. Thus, μ_{f0}^2 was only varied downwards to 1.6 GeV², and the resulting uncertainty on the PDFs was again symmetrised. The suitability of the chosen central parameterisation was re-verified for the new settings for M_c and M_b using the χ^2 saturation method as described in Section 3.1.

Since predictions at NNLO for the jet data were only available in the zero-mass scheme, and results for the treatment of the inclusive data in different VFNS and FFNS schemes were consistent [2], no other heavy-flavour schemes were investigated.

⁴A cross-check was performed with the fixed value of $\alpha_s = 0.118$ and no significant difference in the resulting M_c and M_b values were observed.

⁵In previous HERAPDF analyses, the uncertainty on M_c was large enough to accommodate the upward μ_{f0}^2 variation.

3.4 Hadronisation uncertainties

For the jet-data analysis, it was also necessary to consider hadronisation and the effect of the uncertainties on hadronisation corrections. The uncertainties on the hadronisation corrections, which were supplied in the original publications, were reviewed for this analysis. The H1 uncertainties were used as published, while for technical reasons, those for the ZEUS data were increased to the maximum value quoted in the publications, 2 %. It was checked that this change made no significant difference to any of the results presented below.

In the HERAPDF2.0Jets NLO analysis, hadronisation uncertainties were applied using the offset method, i.e. performing separate fits with the hadronisation corrections set to their maximal and minimal values. This resulted in a hadronisation uncertainty on $\alpha_s(M_Z^2)$ of ± 0.0012 [2].

The current procedure is different from this previously used procedure. The uncertainties on the hadronisation corrections were included as input to the HERAPDF2.0 Jets NNLO fits. They were treated as systematic uncertainties correlated between all data sets. Thus, their contribution became part of the overall experimental, i.e. fit, uncertainties. For fits with fixed $\alpha_s(M_Z^2)$, their contribution was negligible. For fits with free $\alpha_s(M_Z^2)$, their contribution to the experimental uncertainty on $\alpha_s(M_Z^2)$ was ± 0.0006 . This represents a significant reduction of the influence of the hadronisation uncertainties.

4 HERAPDF2.0Jets NNLO – results

4.1 Simultaneous determination of $\alpha_s(M_Z^2)$ and PDFs

Jet-production data are essential for the determination of the strong coupling constant, $\alpha_s(M_Z^2)$. In pQCD fits to inclusive DIS data alone, the gluon PDF is determined via the DGLAP equations, using the observed scaling violations. This results in a strong correlation between the shape of the gluon distribution and the value of $\alpha_s(M_Z^2)$. Data on jet and dijet production cross-sections provide an independent constraint on the gluon distribution and are also directly sensitive to $\alpha_s(M_Z^2)$. Thus, such data are essential for an accurate simultaneous determination of $\alpha_s(M_Z^2)$ and the gluon distribution.

When determining $\alpha_s(M_Z^2)$, it is necessary to consider so-called “scale uncertainties”. They approximate the uncertainty due to the influence of higher orders in the perturbation extension. This uncertainty was evaluated by varying the renormalisation and factorisation scales by a factor of two, both separately and simultaneously⁶, and selecting the maximal positive and negative deviations of the result as the “de facto” scale uncertainty. These were observed for $(2.0\mu_r, 1.0\mu_f)$ and $(0.5\mu_r, 1.0\mu_f)$, respectively.

The HERAPDF2.0Jets NNLO fit with free $\alpha_s(M_Z^2)$ results in

$$\alpha_s(M_Z^2) = 0.1156 \pm 0.0011 \text{ (exp)} \stackrel{+0.0001}{-0.0002} \text{ (model + parameterisation)} \pm 0.0029 \text{ (scale)} , \quad (7)$$

⁶This procedure is often called 9-point variation, where the nine variations are $(0.5\mu_r, 0.5\mu_f)$, $(0.5\mu_r, 1.0\mu_f)$, $(0.5\mu_r, 2.0\mu_f)$, $(1.0\mu_r, 0.5\mu_f)$, $(1.0\mu_r, 1.0\mu_f)$, $(1.0\mu_r, 2.0\mu_f)$, $(2.0\mu_r, 0.5\mu_f)$, $(2.0\mu_r, 1.0\mu_f)$, $(2.0\mu_r, 2.0\mu_f)$.

where “exp” denotes the experimental uncertainty, which was taken as the fit uncertainty, including the contribution from hadronisation uncertainties. The value of $\alpha_s(M_Z^2)$ and the size of the experimental uncertainty were confirmed by the result of a so-called χ^2 scan in $\alpha_s(M_Z^2)$, which is shown in Fig. 2 a). Numerous fits with varying $\alpha_s(M_Z^2)$ were performed and the clear minimum observed in χ^2 coincides with the value of $\alpha_s(M_Z^2)$ determined with the fit. The width of the minimum in χ^2 confirms the fit uncertainty. The combined model and parameterisation uncertainty shown in Fig. 2 a) was determined by performing similar scans, for which the values of the model parameters and the parameterisation were varied as described in Section 3.1.

Figure 2 a) also shows the scale uncertainty, which dominates the uncertainties. The scale uncertainty as listed in Eq. 7 was evaluated under the assumption of 100 % correlated uncertainties between bins and data sets. The previously published result at NLO [2] had scale uncertainties calculated under the assumption of 50 % correlated and 50 % uncorrelated uncertainties between bins and data sets. A strong motivation to determine $\alpha_s(M_Z^2)$ at NNLO was the hope to substantially reduce scale uncertainties. Therefore, the analysis was repeated for these assumptions in order to be able to compare the NNLO to the NLO scale uncertainties. The reevaluated NNLO scale uncertainty of (± 0.0022) is indeed significantly lower than the $(+0.0037, -0.0030)$ previously observed in the HERAPDF2.0Jets NLO analysis.

The HERAPDF2.0Jets NNLO fit with free $\alpha_s(M_Z^2)$ was based on 1363 data points and had a $\chi^2/\text{d.o.f.} = 1614/1348 = 1.197$. This can be compared to the $\chi^2/\text{d.o.f.} = 1363/1131 = 1.205$ for HERAPDF2.0 NNLO based on inclusive data only [2]. The similarity of the $\chi^2/\text{d.o.f.}$ values indicates that the data on jet production do not introduce any additional tension to the fit. The jet data are fully consistent with the inclusive data.

The question whether data with relatively low Q^2 bias the determination of $\alpha_s(M_Z^2)$ arose within the context of the HERAPDF2.0 analysis [2]. Figure 2 b) shows the result of $\alpha_s(M_Z^2)$ scans with Q_{min}^2 for the inclusive data set to 3.5 GeV^2 , 10 GeV^2 and 20 GeV^2 . Clear minima are visible which coincide within uncertainties. Figure 2 c) shows the result of similar scans with only the inclusive data used as input [2]. The inclusive data alone cannot sufficiently constrain $\alpha_s(M_Z^2)$.

It has also been suggested that the use of the A'_g term, in the gluon parameterisation could bias the determination of $\alpha_s(M_Z^2)$. Thus cross-checks were made with two modified gluon parameterisations, $A'_g = 0$ and $xg(x) = A_g x^{B_g} (1 - x)^{C_g}$ as well as the alternative gluon parameterisation, AG [2], for which $A'_g = 0$ and $xg(x) = A_g x^{B_g} (1 - x)^{C_g} (1 + D_g x)$. A value of $\alpha_s(M_Z^2) = 0.1151 \pm 0.0010(\text{exp})$ was obtained for both modifications of the parameterisation, which is in agreement with the result for the standard parameterisation. The value of D_g in the AG parameterisation was consistent with zero. These results demonstrate that the present $\alpha_s(M_Z^2)$ determination is not sensitive to the details of the gluon parameterisation.

The result presented here cannot be directly compared to an H1 result [37] and a result published by the NNLOJET authors and their collaborators [38] because a previous version of the theoretical predictions were used for these analyses. The groups have to tell me what to compare to. I could write something about the same version, but as I expect errata, I would prefer to compare to what will come or has come. Decisions and info during EB meeting, please. The following text is tentative.

Other determinations of $\alpha_s(M_Z^2)$ at NNLO using jet data as published by H1 [37] and NNLOJET authors and their collaborators [38] used fixed PDFs for their fits to determine $\alpha_s(M_Z^2)$.

Therefore, the values of $\alpha_s(M_Z^2)$ should not be directly compared. However, both analyses were performed with a cut on μ of $\mu > 2M_b$, which is quite similar to the $\mu > 10.0$ GeV cut used for this analysis. Thus, the scale uncertainties can be compared. The H1 result is based on H1 data only and the quoted scale uncertainty of ± 0.0042 can be compared to the ± 0.0029 obtained for the analysis presented here based on H1 and ZEUS data. The scale uncertainty published by NNLOjet is ± 0.0036 .

The H1 collaboration provided one simultaneous fit of $\alpha_s(M_Z^2)$ and PDFs, based on H1 inclusive and jet data only, and with $Q_{min}^2 = 10 \text{ GeV}^2$. For comparison, the analysis presented here was modified by also setting $Q_{min}^2 = 10 \text{ GeV}^2$. The value of $\alpha_s(M_Z^2)$ published by H1 is $\alpha_s(M_Z^2) = 0.1142 \pm 0.0011(\text{exp}) \pm 0.0003(\text{model/parameterisation}) \pm 0.0026(\text{scale})$ while the current modified analysis resulted in $\alpha_s(M_Z^2) = 0.1156 \pm 0.0011(\text{exp}) \pm 0.0002(\text{model/parameterisation}) \pm 0.0021(\text{scale})$.

4.2 The PDFs of HERAPDF2.0Jets NNLO obtained for fixed $\alpha_s(M_Z^2)$

The value of $\alpha_s(M_Z^2) = 0.1155$ was used for the determination of the PDFs in the HERAPDF2.0Jets NNLO analysis. The value listed in PDG12 [39], 0.118, which was also the value determined in the HERAPDF2.0Jets NLO analysis, was used for the original HERAPDF2.0 analyses at NNLO based on inclusive data only. Therefore, the PDFs of HERAPDF2.0Jets NNLO are shown in Fig. 3 a) and b) for both, fixed $\alpha_s(M_Z^2) = 0.1155$ and fixed $\alpha_s(M_Z^2) = 0.118$, respectively, together with their uncertainties, at the scale $\mu_f^2 = 10 \text{ GeV}^2$. The uncertainties shown are the experimental, i.e. fit, uncertainties as well as the model and parameterisation uncertainties as defined in Section 3.2. The parameterisation uncertainty dominates the uncertainties and is itself dominated by the introduction of the parameter D_{u_v} as a variation. Details on the two sets of PDFs as released are listed in Appendix A.

As the PDFs were derived with a fixed $\alpha_s(M_Z^2)$ value scale uncertainties on the PDFs were not considered, because, in this case, a quantification of theory uncertainties through a variation of the renormalisation and factorisation scales in the fit becomes questionable. Even after the compensation of explicit scale-dependent terms in the NLO and NNLO coefficients, a variation of the renormalisation scale effectively amounts, in its numerical effect, to a modification of the value of $\alpha_s(M_Z^2)$. Fixing the value of $\alpha_s(M_Z^2)$ externally amounts to forcing the fit away from a local minimum, where a variation of the scales could map out the putative uncertainty from missing higher orders. Therefore, scale variations cannot be used as a proxy for uncertainties on the PDF extraction due to missing higher orders. Nevertheless, a cross-check with scale variations as described in Section 4.1 for the fit with free $\alpha_s(M_Z^2)$ was made. The impact on the resulting PDFs was found to be negligible compared to the other uncertainties presented in Fig. 3.

A comparison between the PDFs obtained for $\alpha_s(M_Z^2) = 0.1155$ and $\alpha_s(M_Z^2) = 0.118$ is provided in Figs. 4 and 5 for the scales $\mu_f = 10 \text{ GeV}^2$ and $\mu_f = M_Z^2$, respectively. Here, only total uncertainties are shown. At the lower scale, a significant difference is observed between the gluon distributions; the distribution for $\alpha_s(M_Z^2) = 0.1155$ is above the distribution for $\alpha_s(M_Z^2) = 0.118$ for x less than $\approx 10^{-2}$. This correlation between the value of $\alpha_s(M_Z^2)$ and the shape of the gluon PDF is as expected from QCD evolution. At the scale of M_Z^2 , the differences become negligible in the visible range of x due to QCD evolution.

A comparison of the PDFs obtained for $\alpha_s(M_Z^2) = 0.118$ by HERAPDF2.0Jets NNLO to the PDFs of HERAPDF2.0 NNLO, based on inclusive data only, is provided in Fig. 6. These two sets of PDFs do not show any significant difference in the central values. However, there is a significant reduction of the uncertainties on the gluon PDFs as shown in Fig. 7 at the scale of $\mu_f = 10 \text{ GeV}^2$ and in Fig. 8 at the scale of $\mu_f = M_Z^2$. The reductions in the uncertainties for HERAPDF2.0Jets NNLO for $\alpha_s(M_Z^2) = 0.1155$ compared to $\alpha_s(M_Z^2) = 0.118$ are shown in Fig. 9 and Fig. 10. At high x and $\mu_f = M_Z^2$, the parameterisation uncertainties become important as can be seen by comparing Fig. 10 b) and 10 c).

The reduction in model and parameterisation uncertainty for $x < 10^{-3}$ compared to HERAPDF2.0 NNLO is mostly due to the improved procedure to estimate this uncertainty. The ranges, in which M_c and M_b were varied were reduced, but this had basically no effect on the uncertainties but for the following effect. As discussed Section 3.3, it was necessary to symmetrise the downward variation of μ_{f0}^2 rather than allowing both upward and downward variations. This had the positive effect of removing a slight double-counting of sources of uncertainty that could not be avoided in the original HERAPDF2.0 NNLO procedure. The reduction in the model and parameterisation uncertainties for $x < 10^{-3}$ is mostly due to this effect, whereas the reduction in experimental as well as model and parameterisation uncertainties for $x > 10^{-3}$ is due to the influence of the jet data. This is also demonstrated in Fig. 11, which shows ratios of uncertainties with respect to the total uncertainties of HERAPDF2.0 NNLO based on inclusive data only. Shown are the contributions of the experimental, the experimental plus model and the experimental plus parameterisation uncertainties to the the total uncertainties of HERAPDF2.0 NNLO and the respective reductions for HERAPDF2.0Jets NNLO. Further such ratio plots are provided in Appendix B.

4.3 Comparisons of HERAPDF2.0Jets NNLO predictions to jet data

Comparisons of the predictions based on HERAPDF2.0Jets NNLO with fixed $\alpha_s(M_Z^2) = 0.1155$ to the data on jet production used as input to the fit are shown in Figs. 12 to 19. Each figure presents in a) a direct comparison of the cross sections and in b) the respective ratios.

The uncertainties on the NNLO predictions as provided by `applfast` were taken into account in all HERAPDF2.0Jets NNLO fits. The predictions based on the HERAPDF2.0Jets NNLO PDFs were computed using the assumption of massless jets, i.e. the transverse energy, E_T , and the transverse momentum of a jet, p_T , were assumed to be equivalent. For the inclusive jet analyses, each jet p_T was entered separately. For dijet analyses, the average of the transverse momenta, $\langle p_T \rangle$ was used. In these cases, $\langle p_T \rangle$ was also used to set the factorisation and renormalisation scales to $\mu_f^2 = \mu_r^2 = Q^2 + \langle p_T \rangle^2$ for calculating predictions. Scale uncertainties were not considered [16] for the comparisons to data. The predictions based on the PDFs of HERAPDF2.0Jets NNLO clearly fit the data on jet production used as input very well, showing that the inclusive data and jet production data both used as input to the NNLO QCD fit are fully consistent.

5 Summary

The HERA data set on inclusive ep scattering as published by the H1 and ZEUS collaborations [2], together with selected data on jet production, published separately by the two collab-

orations, were used as input to a pQCD analysis at NNLO.

An analysis was performed where $\alpha_s(M_Z^2)$ and the PDFs were fitted simultaneously. This resulted in a value of $\alpha_s(M_Z^2) = 0.1156 \pm 0.0011$ (exp) $^{+0.0001}_{-0.0002}$ (model/ /parameterisation) ± 0.0029 (scale). This result on $\alpha_s(M_Z^2)$ is compatible with the world average [40] and it is competitive in comparison with other determinations at NNLO. The scale uncertainties were calculated under the assumption of fully correlated uncertainties between bins and data sets. They would decrease to ± 0.0021 under the assumption of 50 % correlated and 50 % uncorrelated uncertainties which is the value that can be directly compared to the previously published [2] scale uncertainties of (+0.0037,-0.0030) observed in the HERAPDF2.0Jets NLO analysis.

Two sets of PDFs were determined for HERAPDF2.0Jets NNLO for fixed $\alpha_s(M_Z^2) = 0.1155$ and $\alpha_s(M_Z^2) = 0.118$. They are available to the community. Comparisons between the PDFs of HERAPDF2.0Jets NNLO obtained for the two values of $\alpha_s(M_Z^2)$ were shown, as well as comparisons to HERAPDF2.0 NNLO, for which jet data were not used as input to the fit. All these PDFs are very similar, showing the consistency of the inclusive and the jet production data. On balance, the inclusion of the jet data had two consequences: i) a lower value of $\alpha_s(M_Z^2)$ is favoured; ii) the uncertainty on the gluon PDF was reduced. Predictions based on the PDFs of HERAPDF2.0Jets NNLO were compared to the jet production data used as input. The predictions describe the data very well.

The PDFs of HERAPDF2.0Jets NNLO complete the HERAPDF2.0 ensemble of parton distribution functions. This ensemble of PDFs, extracted from HERA data alone, presents a consistent picture in the framework of pQCD. It is one of the legacies of HERA.

6 Acknowledgements

We are grateful to the HERA machine group whose outstanding efforts have made the H1 and ZEUS experiments possible. We appreciate the contributions to the construction, maintenance and operation of the H1 and ZEUS detectors of many people who are not listed as authors. We thank our funding agencies for financial support, the DESY technical staff for continuous assistance and the DESY directorate for their support and for the hospitality they extended to the non-DESY members of the collaborations. We would like to give credit to all partners contributing to the EGI computing infrastructure for their support. We acknowledge the support of the IPPP Associateship program for this project.

References

- [1] A. Cooper-Sarkar and R. Devenish, *Deep inelastic Scattering*, Oxford Univ. Press (2011), ISBN 978-0-19-960225-4.
- [2] H. Abramowicz *et al.*, [H1 and ZEUS Collaborations], *Eur. Phys. J. C* **75**, 580 (2015), [arXiv:1506.06042].
- [3] V. N. Gribov and L. N. Lipatov, *Sov. J. Nucl. Phys.* **15**, 438 (1972).
- [4] V. N. Gribov and L. N. Lipatov, *Sov. J. Nucl. Phys.* **15**, 675 (1972).
- [5] L. N. Lipatov, *Sov. J. Nucl. Phys.* **20**, 94 (1975).
- [6] Y. L. Dokshitzer, *Sov. Phys. JETP* **46**, 641 (1977).
- [7] G. Altarelli and G. Parisi, *Nucl. Phys. B* **126**, 298 (1977).
- [8] B. Fanchiotti, S. Kniehl and A. Sirlin, *Phys. Rev. D* **48**, 307 (1993), [hep-ph/9803393].
- [9] A. Aktas *et al.* [H1 Collaboration], *Phys. Lett. B* **653**, 134 (2007), [arXiv:0706.3722].
- [10] F. Aaron *et al.* [H1 Collaboration], *Eur. Phys. J. C* **67**, 1 (2010), [arXiv:0911.5678].
- [11] S. Chekanov *et al.* [ZEUS Collaboration], *Phys. Lett. B* **547**, 164 (2002), [hep-ex/0208037].
- [12] H. Abramowicz *et al.* [ZEUS Collaboration], *Eur. Phys. J. C* **70**, 965 (2010), [arXiv:1010.6167].
- [13] V. Andreev *et al.* [H1 Collaboration], *Eur. Phys. J. C* **77**, 215 (2017), [arXiv:1611.03421].
- [14] V. Andreev *et al.* [H1 Collaboration], *Eur. Phys. J. C* **65**, 2 (2015), [arXiv:1406.4709].
- [15] J. Currie, T. Gehrmann, and J. Niehues, *Phys. Rev. Lett.* **117**, 042001 (2016), [arXiv:1606.03991].
- [16] J. Currie, T. Gehrmann, A. Huss, and J. Niehues, *JHEP* **1707**, 018 (2017), [arXiv:1703.05977].
- [17] T. Gehrmann *et al.*, in *The Proceedings of the 13th International Symposium on Radiative Corrections (RADCOR2017)*, St.Gilgen, Austria (2017), vol. 1707, [arXiv:1801.06415].
- [18] T. Kluge, K. Rabbertz, and M. Wobisch (2006), [hep-ph/0609285].
- [19] Britzger.D *et al.*, in *20th International Workshop on Deep-Inelastic Scattering and Related Subjects (DIS 2012): Bonn, Germany* (2012), p. 217, [arXiv:1208.3641].
- [20] D. Britzger *et al.*, at *DIS 2014* (2014), URL <http://indico.cern.ch/event/258017/session/1/contribution/202>.
- [21] T. Carli, G. Salam, and F. Siegert (2005), [arXiv:0510324].
- [22] T. Carli *et al.*, *Eur. Phys. J. C* **66**, 503 (2010), [arXiv:0911.2985].

- [23] V. Andreev *et al.* [H1 Collaboration], Eur. Phys. J. C **77**, 791 (2017).
- [24] S. Forte and Z. Kassabov, Eur. Phys. J. C **80**, 182 (2020), [arXiv:2001.04986].
- [25] R. S. Thorne and R. G. Roberts, Phys. Rev. D **57**, 6871 (1998), [hep-ph/9709442].
- [26] R. S. Thorne, Phys. Rev. D **73**, 054019 (2006), [hep-ph/0601245].
- [27] R. S. Thorne, Phys. Rev. D **86**, 074017 (2012), [arXiv:1201.6180].
- [28] H. Abramowicz *et al.*, [H1 and ZEUS Collaborations], Eur. Phys. J. C **78**, 473 (2018), [arXiv:1804.01019].
- [29] F. D. Aaron *et al.*, [H1 and ZEUS Collaborations], Eur. Phys. J. C **73**, 2311 (2013), [arXiv:1211.1182].
- [30] M. Botje, Comp. Phys. Comm. **182**, 490 (2011), [arXiv:1005.1481].
- [31] S. Alekhin *et al.* (2014), [arXiv:1410.4412].
- [32] H. Spiesberger, in *Proc. of Future Physics at HERA*, edited by G. Ingelman, A. De Roeck and R. Klanner (1995), p. 227.
- [33] F. Aaron *et al.*, [H1 and ZEUS Collaborations], JHEP **1001**, 109 (2010), [arXiv:0911.0884].
- [34] A. D. Martin, W. J. Stirling, R. S. Thorne, and G. Watt, Eur. Phys. J. C **63**, 189 (2009), [arXiv:0901.0002].
- [35] P. M. Nadolsky *et al.*, Phys. Rev. D **78**, 013004 (2008), [arXiv:0802.0007].
- [36] M. Aaboud *et al.*, Eur. Phys. J. C **77**, 367 (2017), [arXiv:1612.03016].
- [37] V. Andreev *et al.* [H1 Collaboration], Eur. Phys. J. C **77**, 791 (2019), [arXiv:1709.07251].
- [38] D. Britzger *et al.* [NNLOJet and Applfast Collaboration], Eur. Phys. J. C **79**, 845 (2019), [arXiv:1906.05303].
- [39] J. Beringer *et al.* (Particle Data Group), Phys. Rev. D **86**, 010001 (2012).
- [40] M. Tanabashi *et al.* (Particle Data Group), Phys. Rev. D **98**, 030001 (2018).
- [41] The combined data together with the full correlation information and the grids for HERA-PDF2.0 are provided at URL <http://www.desy.de/h1zeus/herapdf20/>.

Data Set	taken from to	$Q^2[\text{GeV}^2]$ range from to	\mathcal{L} pb^{-1}	e^+/e^-	\sqrt{s} GeV	normalised	all points	used points	Ref.
H1 HERA I normalised jets	1999 – 2000	150 15000	65.4	e^+p	319	yes	24	24	[9]
H1 HERA I jets at low Q^2	1999 – 2000	5 100	43.5	e^+p	319	no	28	20	[10]
H1 normalised inclusive jets at high Q^2	2003 – 2007	150 15000	351	e^+p/e^-p	319	yes	30	30	[13,14]
H1 normalised dijets at high Q^2	2003 – 2007	150 15000	351	e^+p/e^-p	319	yes	24	24	[14]
H1 normalised inclusive jets at low Q^2	2005 – 2007	5.5 80	290	e^+p/e^-p	319	yes	48	37	[13]
H1 normalised dijets at low Q^2	2005 – 2007	5.5 80	290	e^+p/e^-p	319	yes	48	37	[13]
ZEUS inclusive jets	1996 – 1997	125 10000	38.6	e^+p	301	no	30	30	[11]
ZEUS dijets	1998 – 2000 & 2004 – 2007	125 20000	374	e^+p/e^-p	318	no	22	16	[12]

Table 1: The data sets on jet production from H1 and ZEUS used for the HERAPDF2.0Jets NNLO its. The term normalised indicates that all cross sections are normalised to the respective NC inclusive cross sections.

Parameter	Central Value	Downwards variation	Upwards variation
Q_{min}^2 [GeV ²]	3.5	2.5	5.0
f_s	0.4	0.3	0.5
M_c [GeV]	1.41	1.37*	1.45
M_b [GeV]	4.20	4.10	4.30
μ_{f0}^2 [GeV ²]	1.9	1.6	2.2*

Table 2: Central values of model input parameters and their one-sigma variations. It was not possible to implement the variations marked * because $\mu_{f0} < M_c$ is required, see Section 3.3. In these cases, the uncertainty on the PDF obtained from the other variation was symmetrised.

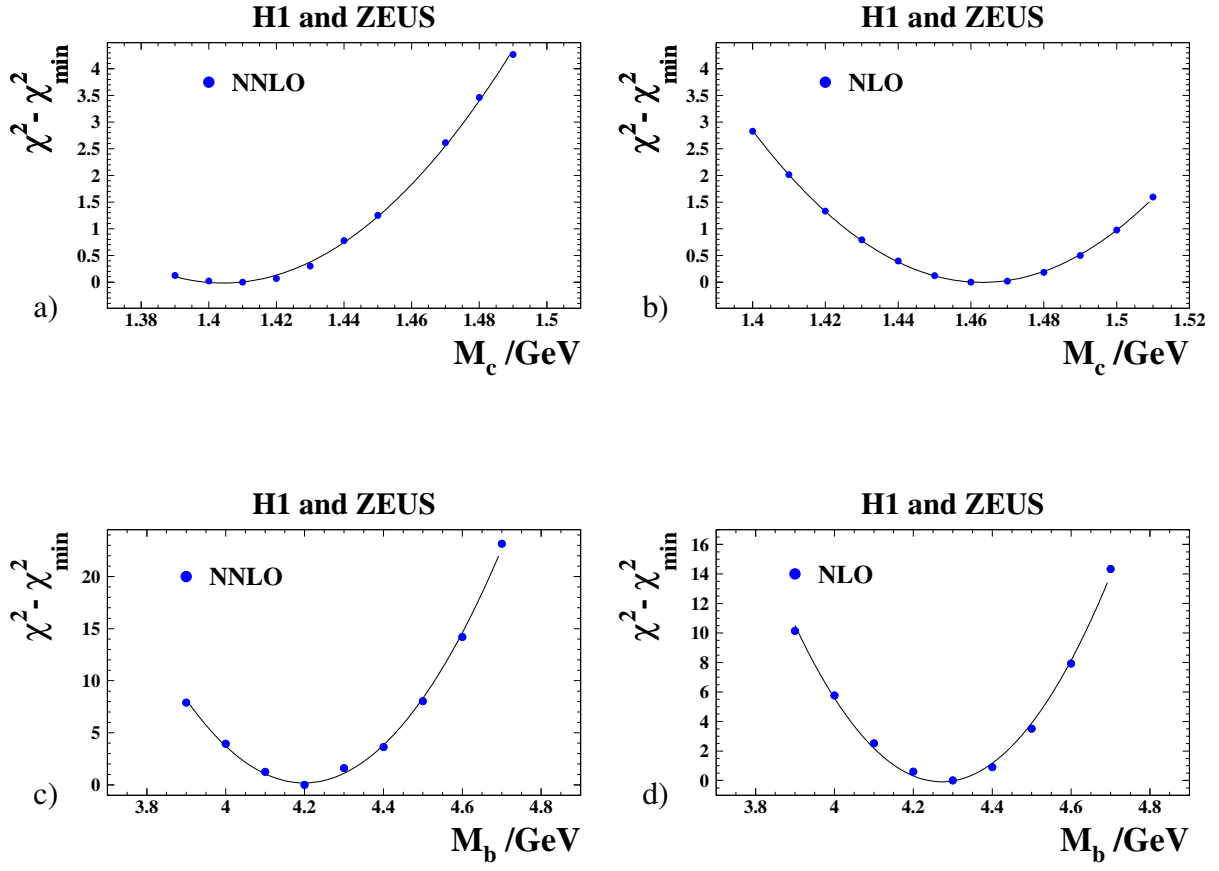


Figure 1: $\Delta\chi^2 = \chi^2 - \chi^2_{\min}$ vs. a) and b) M_c with $M_b = 4.2$ GeV, and c) and d) M_b with $M_c = 1.41$ GeV for a) and c) HERAPDF2.0Jets NNLO fits with fixed $\alpha_s(M_Z^2) = 0.1155$ and the corresponding NLO fits for $M_c = 1.46$ GeV, $M_b = 4.3$ GeV and $\alpha_s(M_Z^2) = 0.118$.

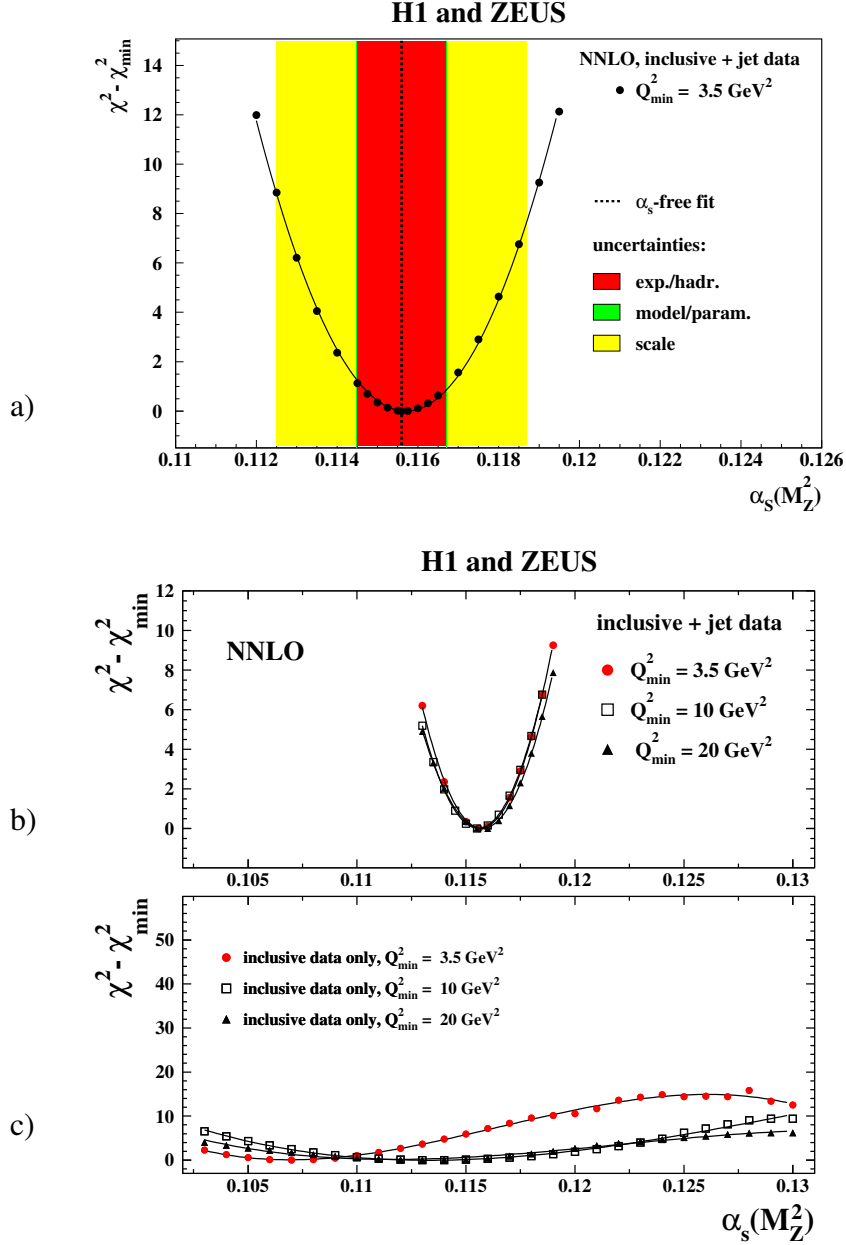


Figure 2: $\Delta\chi^2 = \chi^2 - \chi_{\min}^2$ vs. $\alpha_s(M_Z^2)$ for HERAPDF2.0Jets NNLO fits with fixed $\alpha_s(M_Z^2)$ with a) the standard Q_{\min}^2 of 3.5 GeV^2 b) with Q_{\min}^2 set to 3.5 GeV^2 , 10 GeV^2 and 20 GeV^2 for the inclusive data. In a), the result and all uncertainties determined for the HERAPDF2.0Jets NNLO fit with free $\alpha_s(M_Z^2)$ are also shown, added in quadrature. In b), not all scan points for Q_{\min}^2 of 3.5 GeV^2 are plotted for better visibility. c) For comparison, the situation for fits to only inclusive data is shown, taken from [2].

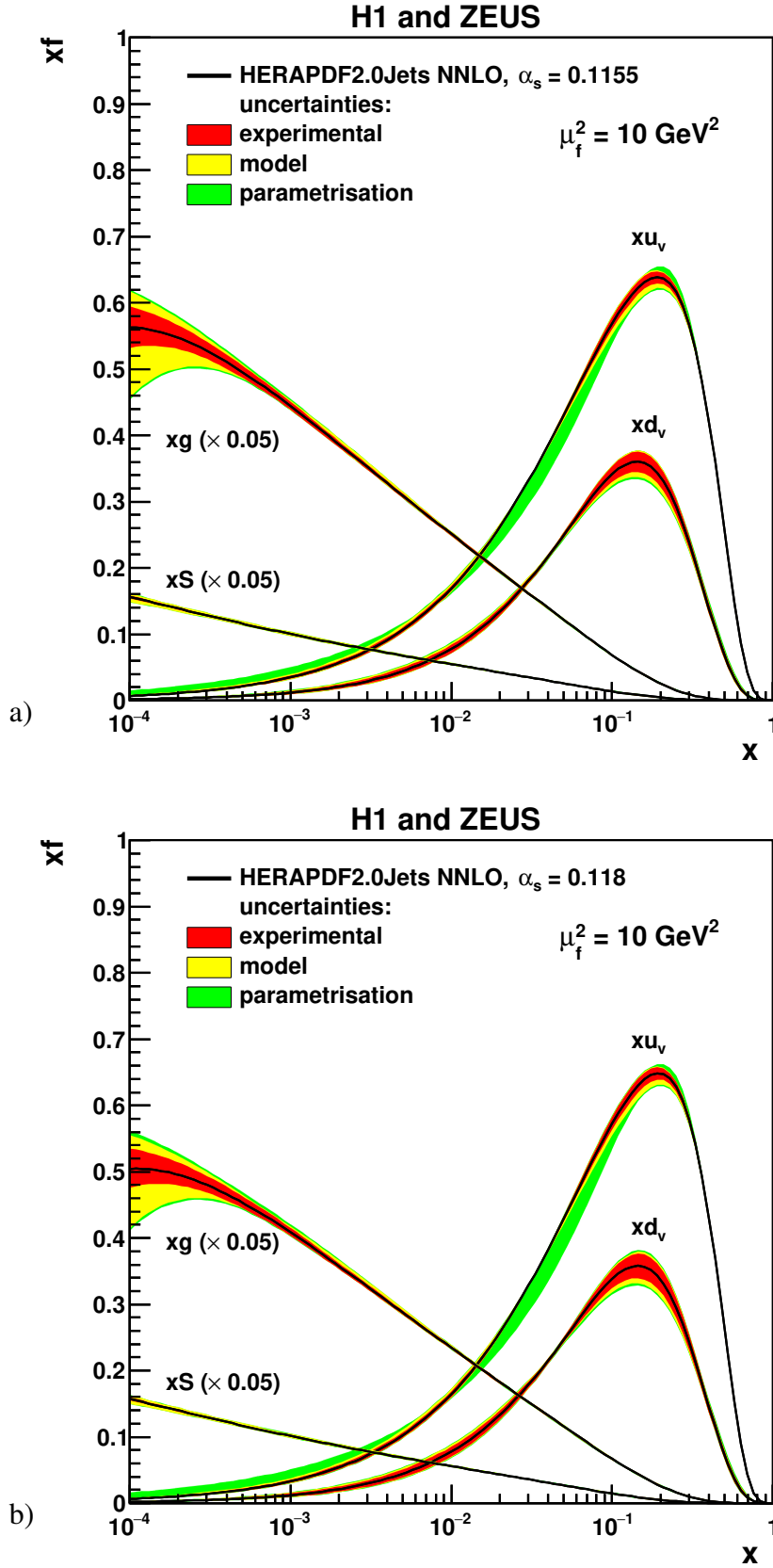


Figure 3: The parton distribution functions xu_v , xd_v , xg and $xS = x(\bar{U} + \bar{D})$ of HERAPDF2.0Jets NNLO, with a) $\alpha_s(M_Z^2)$ fixed to 0.1155 and b) $\alpha_s(M_Z^2)$ fixed to 0.118 at the scale $\mu_f^2 = 10 \text{ GeV}^2$. The uncertainties are shown as differently shaded bands.

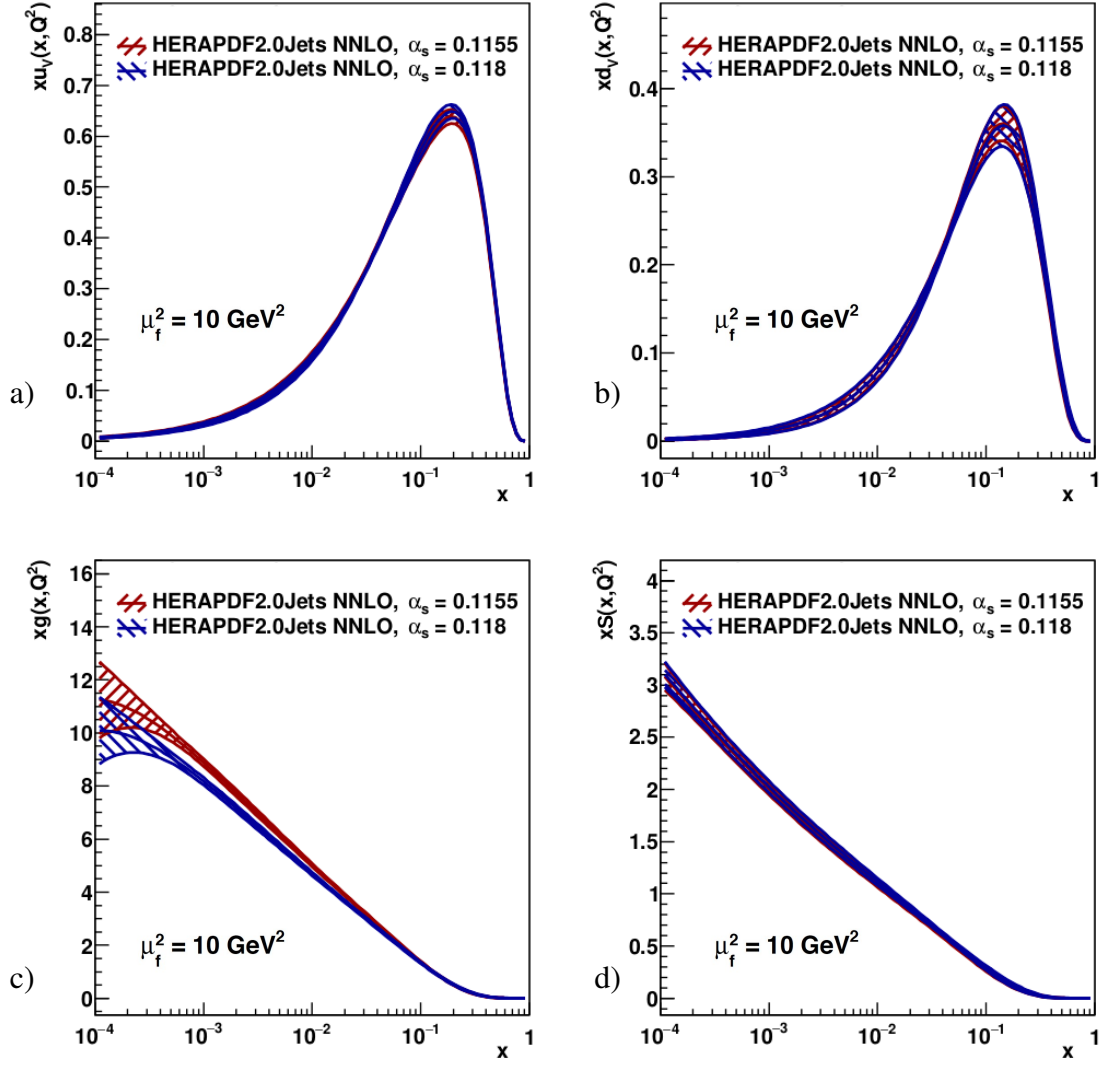


Figure 4: Comparison of the parton distribution functions a) xu_v , b) xd_v , c) xg and d) $xS = x(\bar{U} + \bar{D})$ of HERAPDF2.0Jets NNLO with fixed $\alpha_s(M_Z^2) = 0.1155$ and $\alpha_s(M_Z^2) = 0.118$ at the scale $\mu_f^2 = 10 \text{ GeV}^2$. The total uncertainties are shown as differently hatched bands.

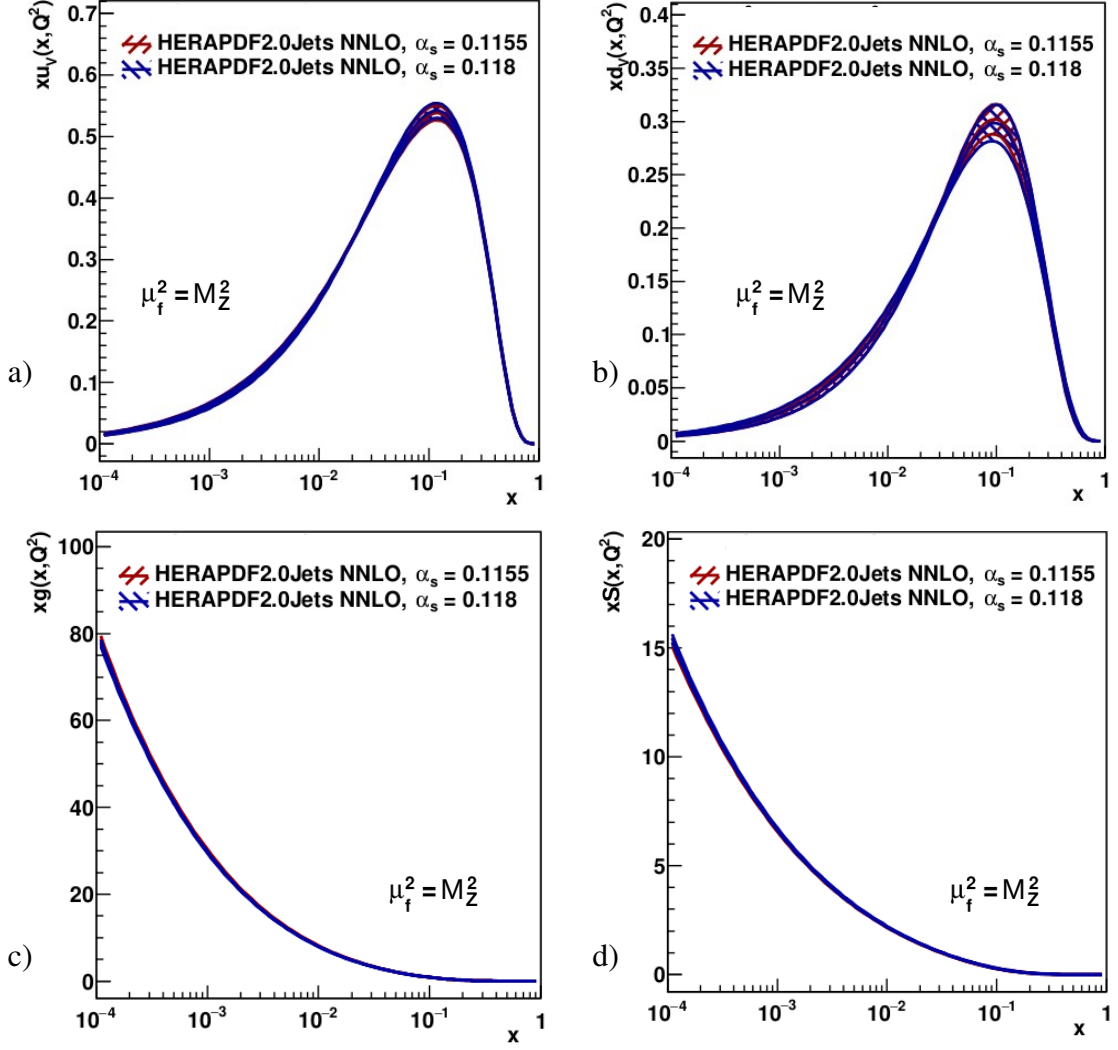


Figure 5: Comparison of the parton distribution functions a) xu_v , b) xd_v , c) xg and d) $xS = x(\bar{U} + \bar{D})$ of HERAPDF2.0Jets NNLO with fixed $\alpha_s(M_Z^2) = 0.1155$ and $\alpha_s(M_Z^2) = 0.118$ at the scale $\mu_f^2 = M_Z^2$ with $M_Z = 91.19$ GeV [40]. The total uncertainties are shown as differently hatched bands.

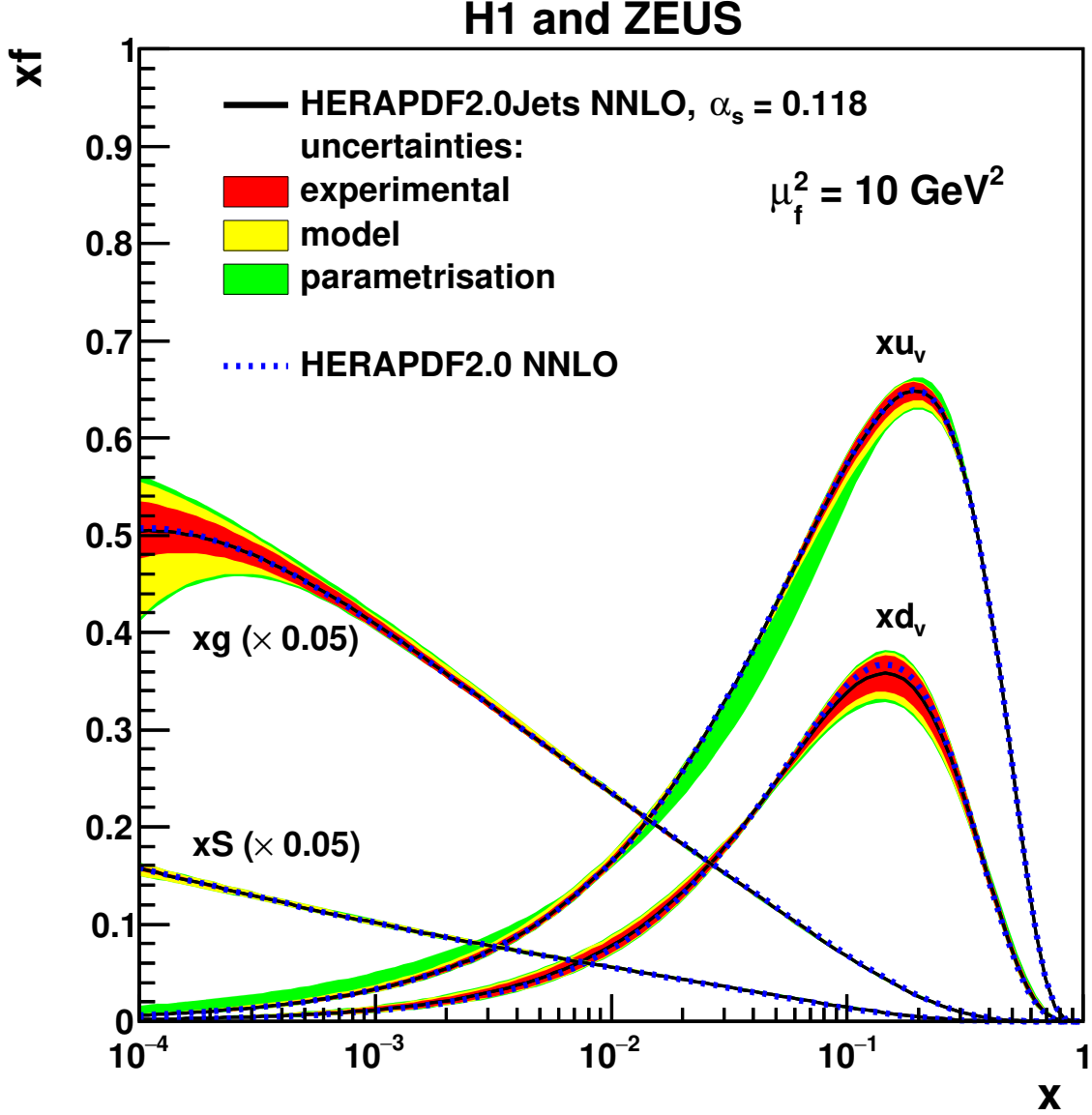


Figure 6: Comparison of the parton distribution functions xu_v , xd_v , xg and $xS = x(\bar{U} + \bar{D})$ of HERAPDF2.0Jets NNLO and HERAPDF2.0 NNLO, which was based on inclusive data only, both with fixed $\alpha_s(M_Z^2) = 0.118$, at the scale $\mu_f^2 = 10 \text{ GeV}^2$. The full uncertainties of HERAPDF2.0Jets NNLO are shown as differently shaded bands and the central value of HERAPDF2.0 NNLO is shown as a dotted line.

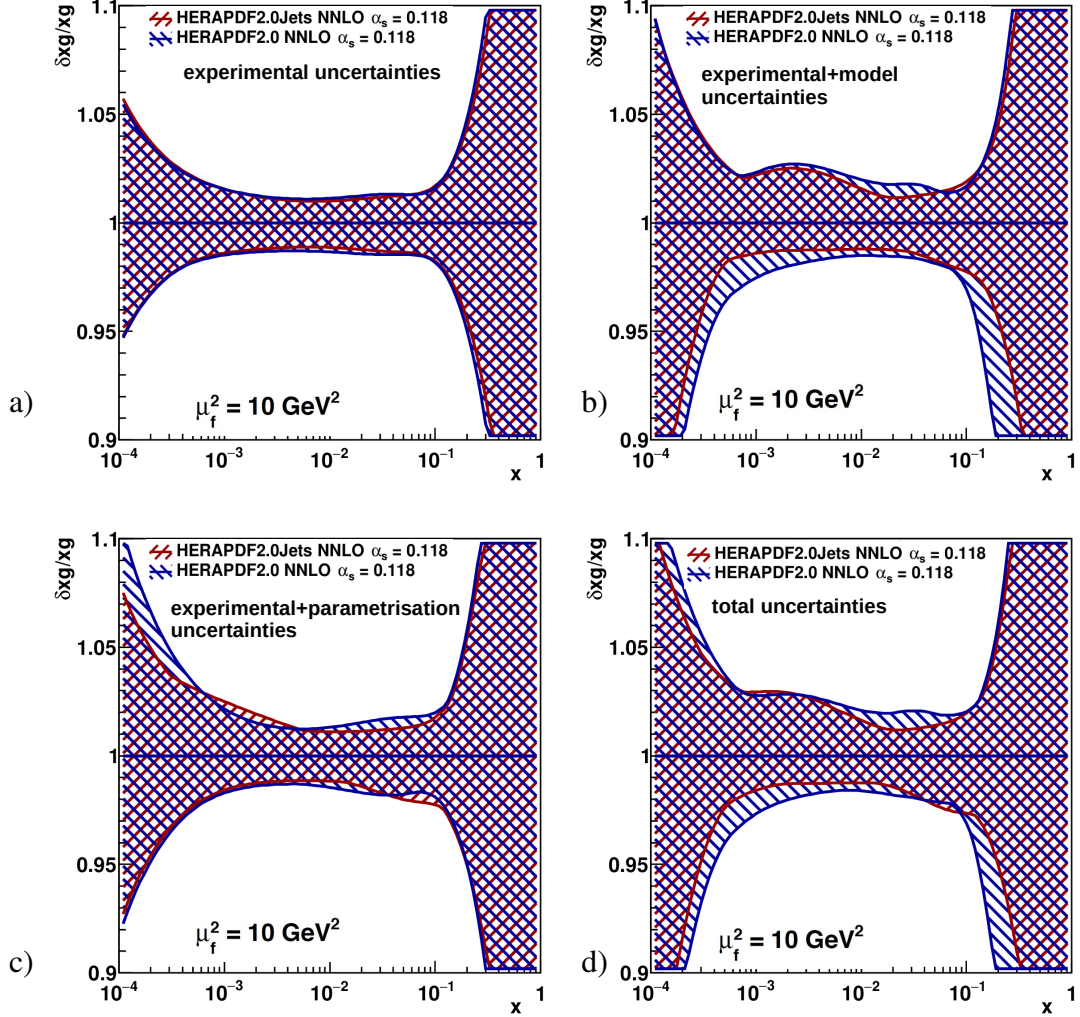


Figure 7: Comparison of the normalised uncertainties on the gluon PDFs of HERAPDF2.0Jets NNLO and HERAPDF2.0 NNLO for a) experimental, i.e. fit, b) experimental plus model, c) experimental plus parameterisation, d) total uncertainties at the scale $\mu_f^2 = 10 \text{ GeV}^2$. The uncertainties on both gluon distributions are shown as differently hatched bands.

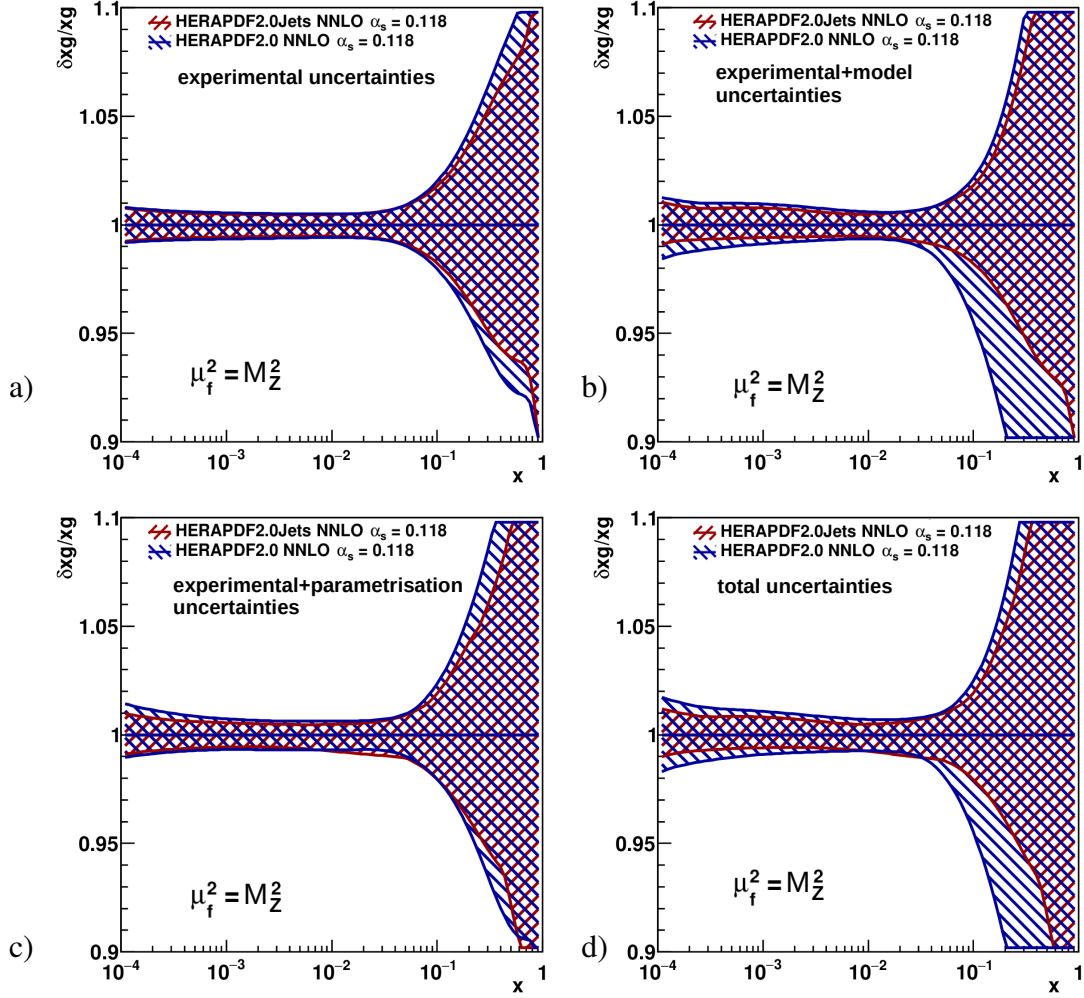


Figure 8: Comparison of the normalised uncertainties on the gluon PDFs of HERAPDF2.0Jets NNLO and HERAPDF2.0 NNLO for a) experimental, i.e. fit, b) experimental plus model, c) experimental plus parameterisation, d) total uncertainties at the scale $\mu_f^2 = M_Z^2$. The uncertainties on both gluon distributions are shown as differently hatched bands.

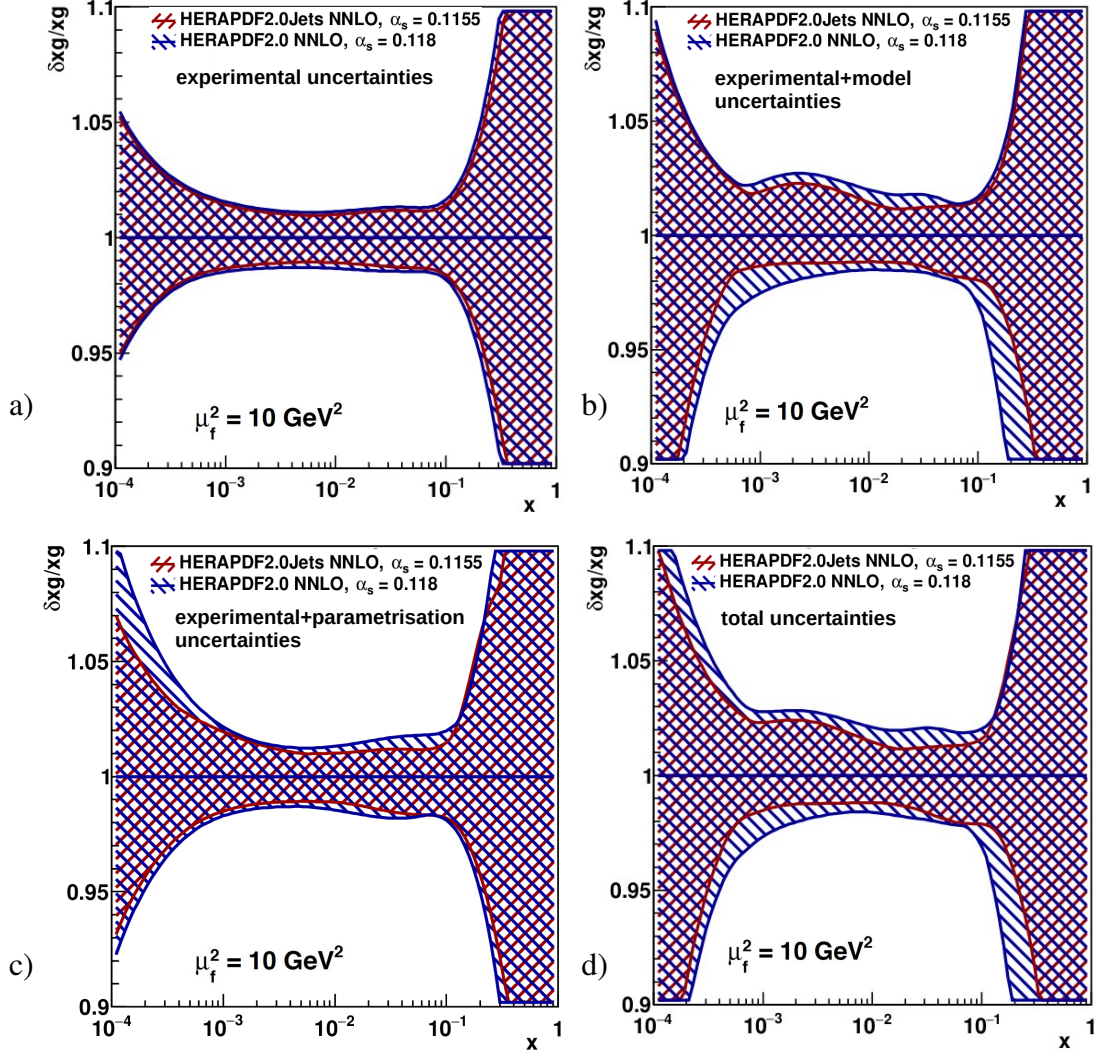


Figure 9: Comparison of the normalised uncertainties on the gluon PDFs of HERAPDF2.0Jets NNLO and HERAPDF2.0 NNLO for a) experimental, i.e. fit, b) experimental plus model, c) experimental plus parameterisation, d) total uncertainties at the scale $\mu_f^2 = 10 \text{ GeV}^2$. The uncertainties on both gluon distributions are shown as differently hatched bands.

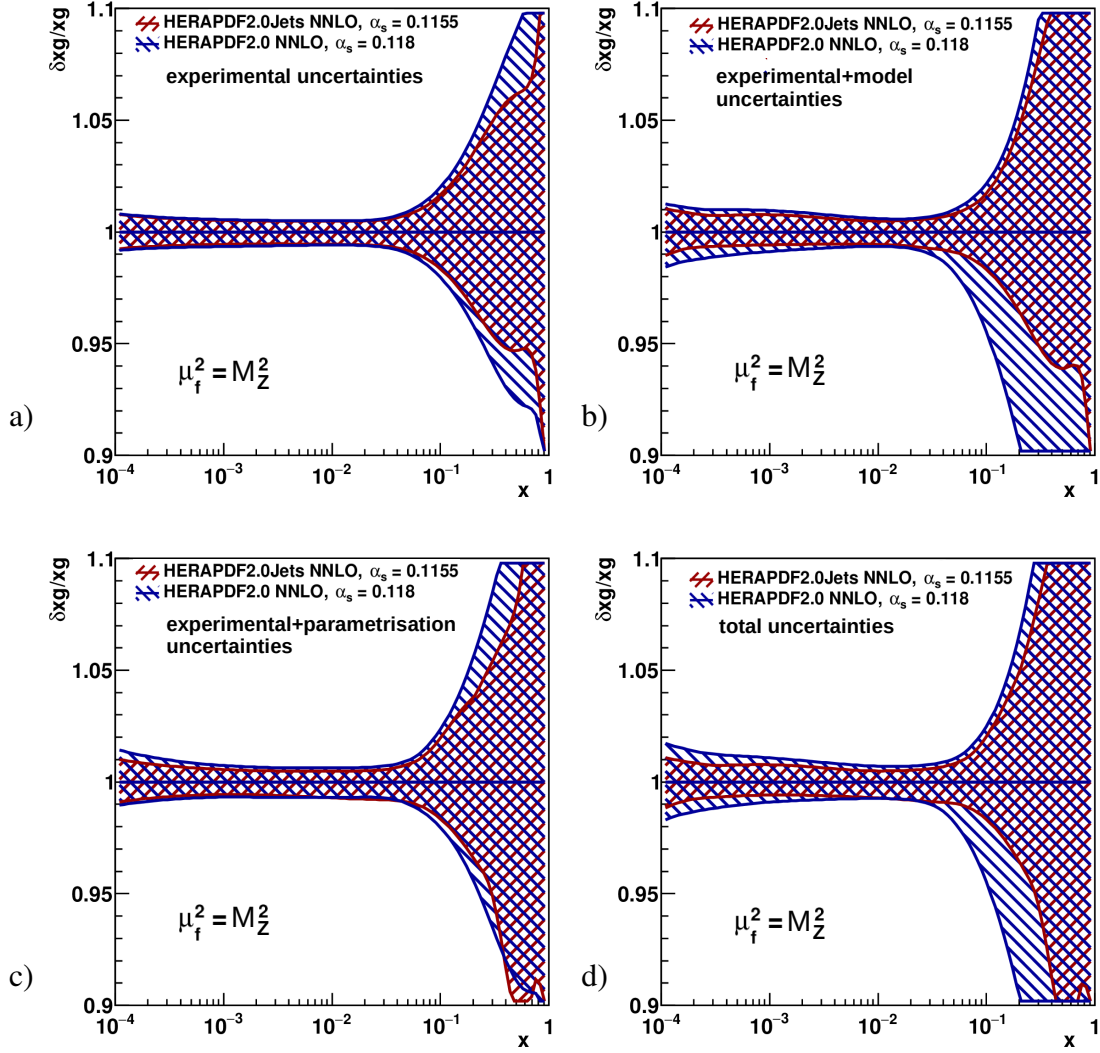


Figure 10: Comparison of the normalised uncertainties on the gluon PDFs of HERAPDF2.0Jets NNLO and HERAPDF2.0 NNLO for a) experimental, i.e. fit, b) experimental plus model, c) experimental plus parameterisation, a) total uncertainties at the scale $\mu_f^2 = M_Z^2$. The uncertainties on both gluon distributions are shown as differently hatched bands.

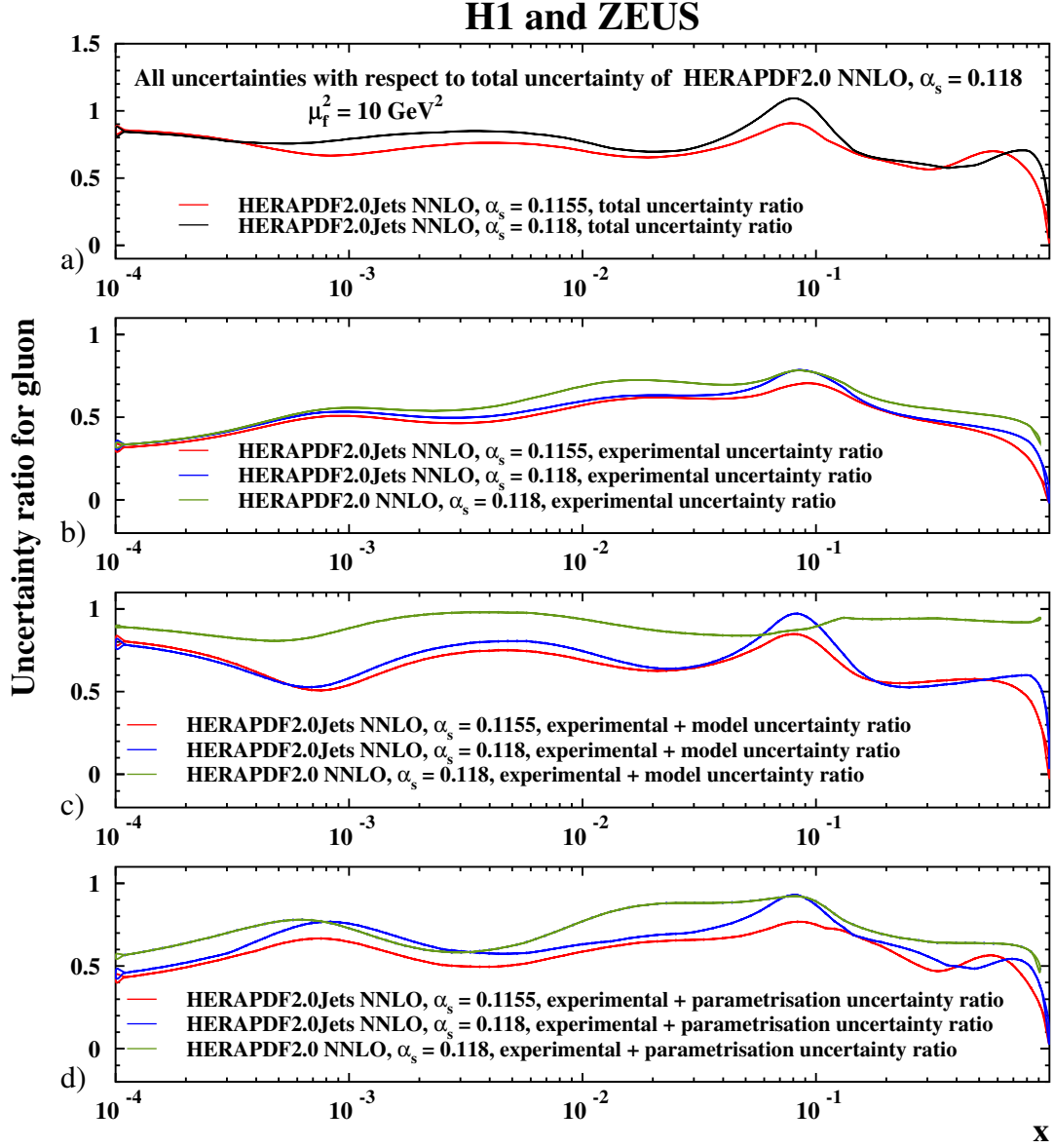


Figure 11: Ratios of uncertainties relative to the total uncertainties of HERAPDF2.0 NNLO $\alpha_s(M_Z^2) = 0.118$ a) total, b) experimental, c) experimental plus model, d) experimental plus parameterisation uncertainties for HERAPDF2.0Jets NNLO $\alpha_s(M_Z^2) = 0.118$ and $\alpha_s(M_Z^2) = 0.1155$ at the scale $\mu_f^2 = 10 \text{ GeV}^2$.

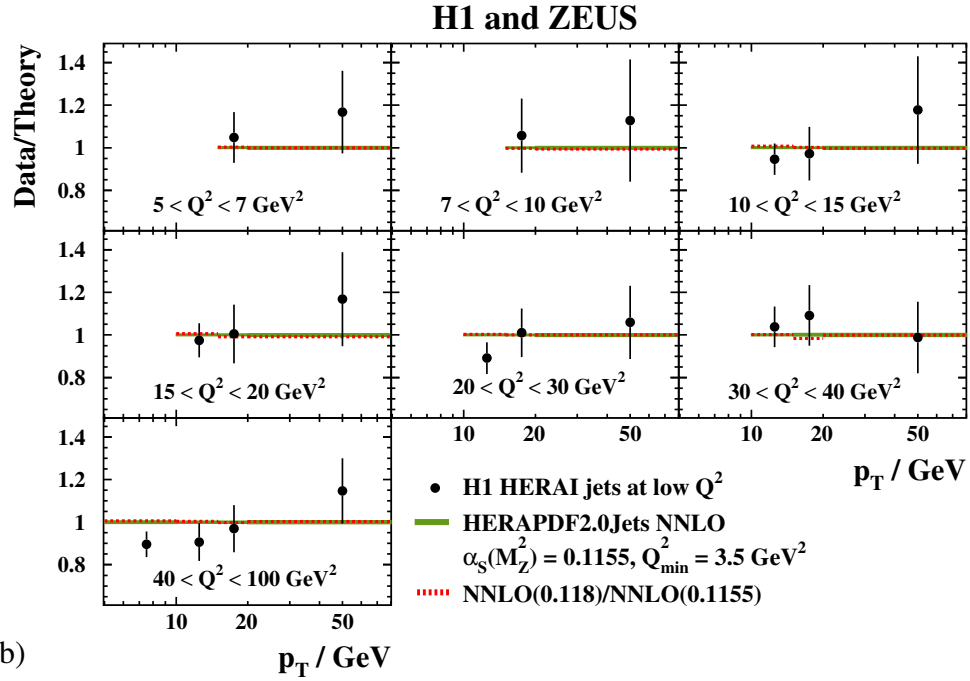
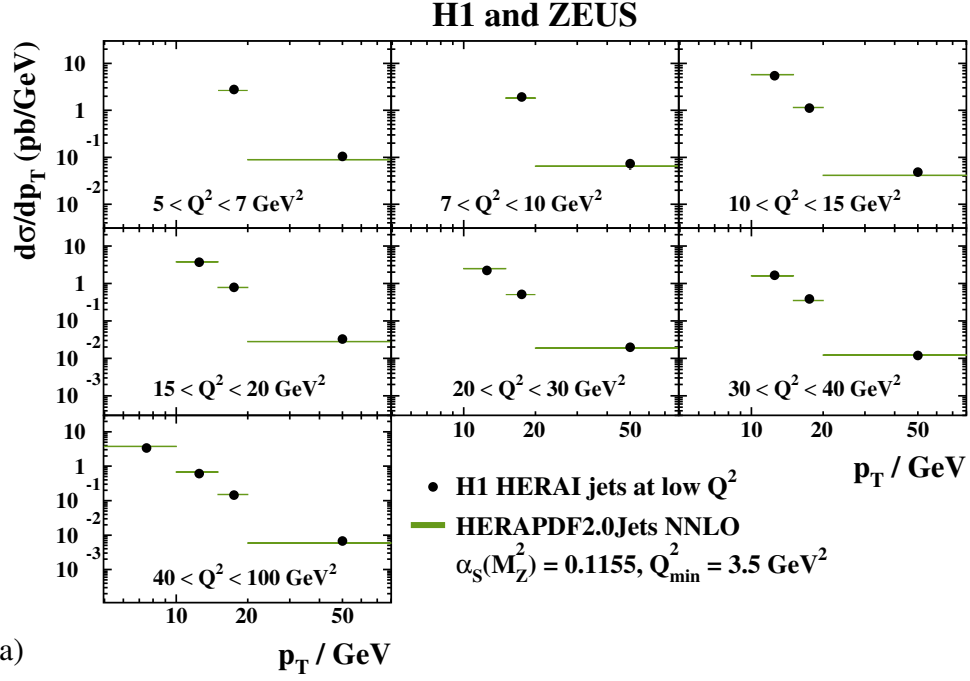


Figure 12: a) Differential jet cross sections, $d\sigma/dp_T$, in bins of Q^2 between 5 and 100 GeV^2 as measured by H1. Also shown are predictions based on HERAPDF2.0Jets NNLO. The bands represent the total uncertainties on the predictions excluding scale uncertainties, the bands are mostly invisible. Only data used in the fit are shown. b) Measured cross sections divided by predictions based on HERAPDF2.0Jets NNLO.

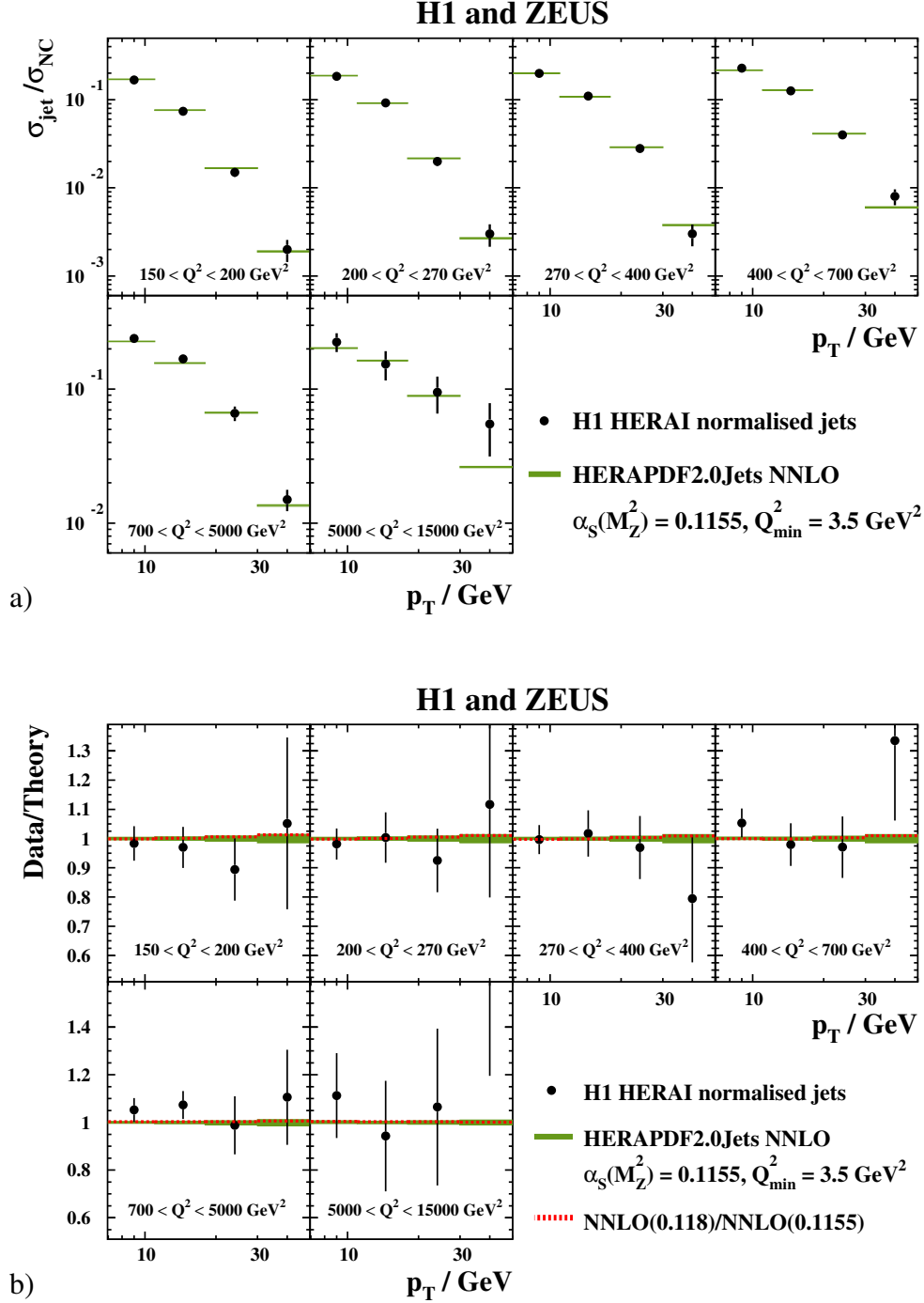


Figure 13: a) Differential jet cross sections, $d\sigma/dp_T$, normalised to NC inclusive cross sections, in bins of Q^2 between 150 and 15000 GeV^2 as measured by H1. Also shown are predictions based on HERAPDF2.0Jets NNLO. The bands represent the total uncertainties on the predictions excluding scale uncertainties; the bands are mostly invisible. Only data used in the fit are shown. b) Measured cross sections divided by predictions based on HERAPDF2.0Jets NNLO.

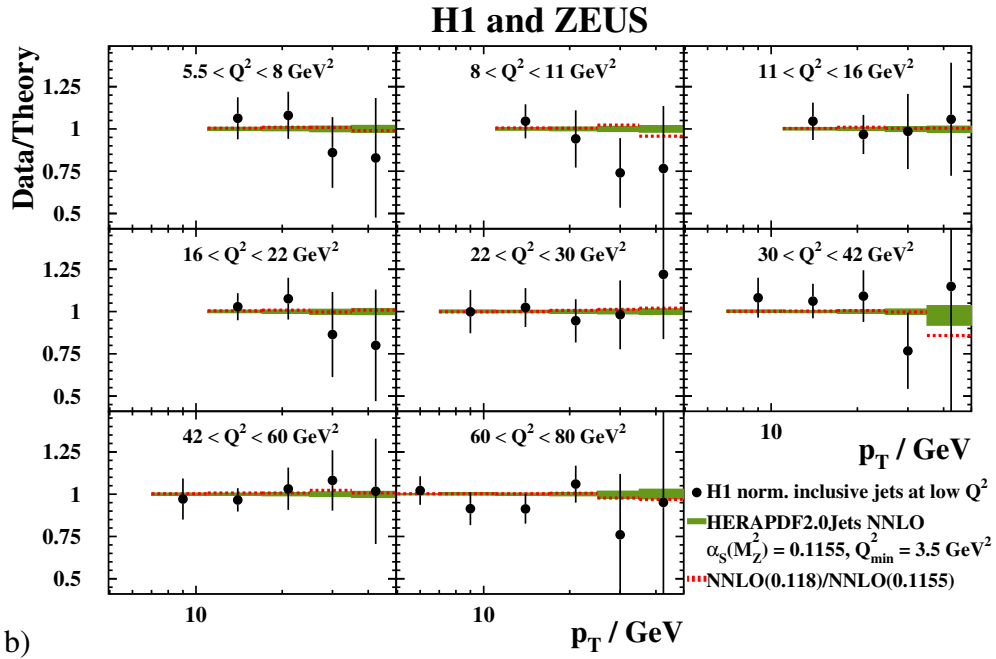
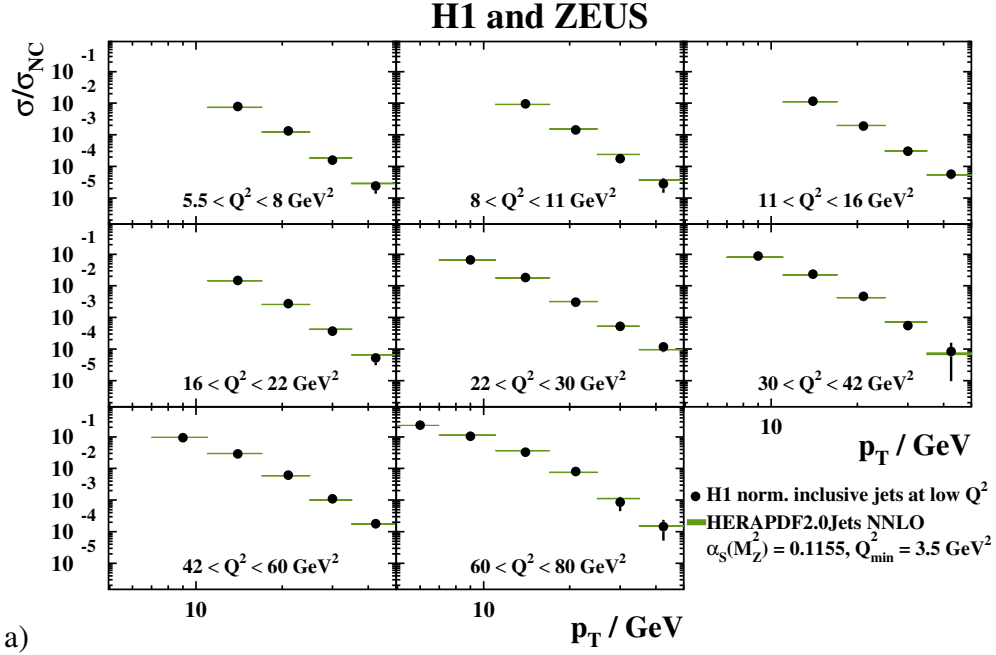


Figure 14: a) Differential inclusive jet cross sections, $d\sigma/dp_T$, normalised to NC inclusive cross sections, in bins of Q^2 between 5 and 80 GeV^2 as measured by H1. Also shown are predictions based on HERAPDF2.0Jets NNLO. The bands represent the total uncertainties on the predictions excluding scale uncertainties; the bands are mostly invisible. Only data used in the fit are shown. b) Measured cross sections divided by predictions based on HERAPDF2.0Jets NNLO.

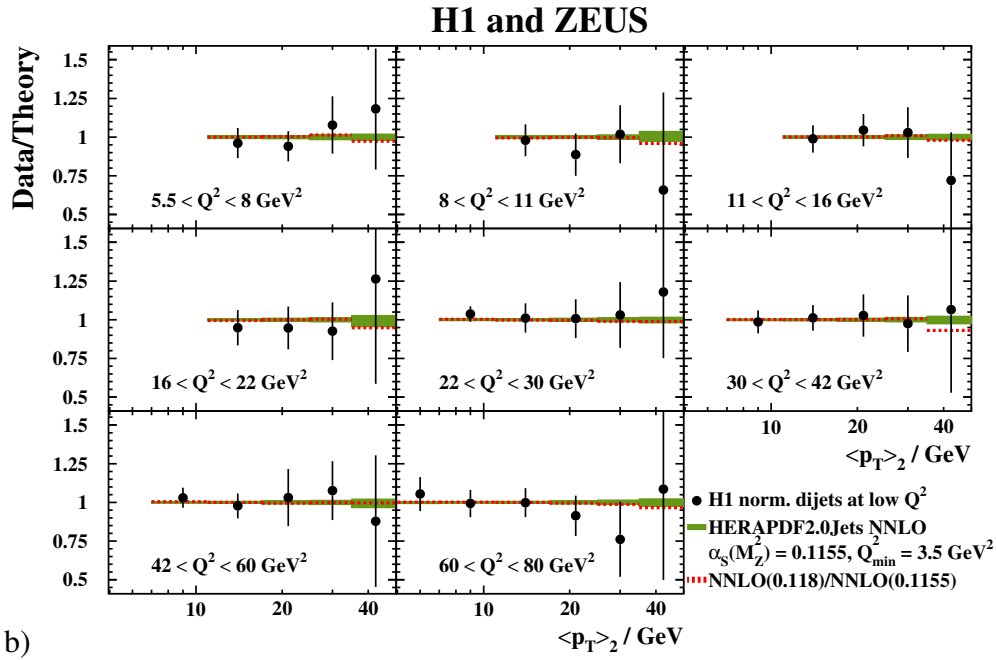
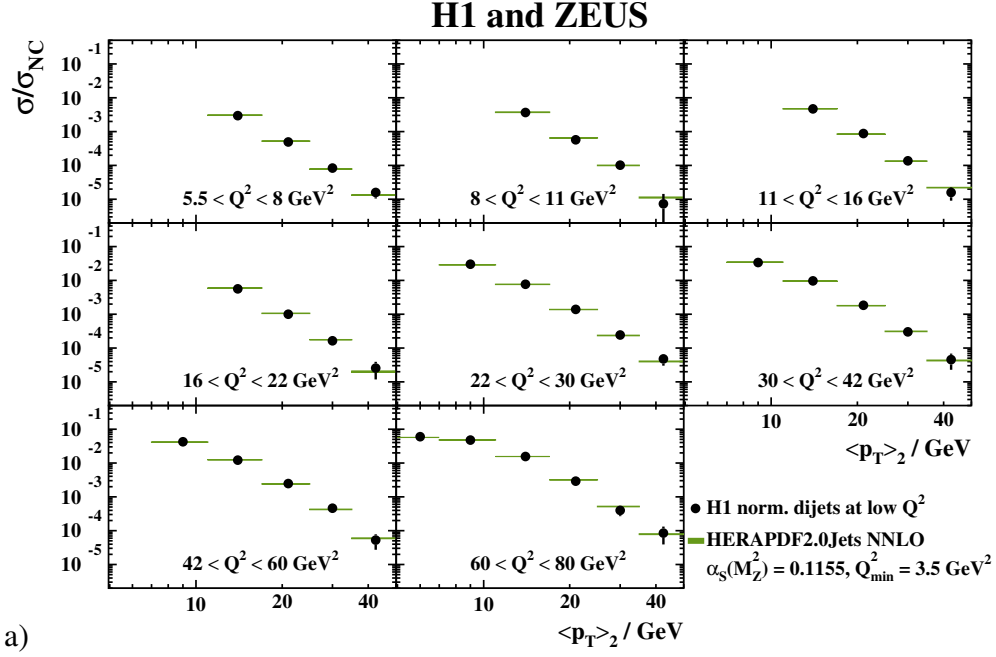


Figure 15: a) Differential dijet normalised cross sections, $d\sigma/d\langle p_T \rangle_2$, normalised to NC inclusive cross sections, in bins of Q^2 between 5 and 80 GeV^2 as measured by H1. The variable $\langle p_T \rangle_2$ denotes the average p_T of the two jets. Also shown are predictions based on HERAPDF2.0Jets NNLO. The bands represent the total uncertainties on the predictions excluding scale uncertainties; the bands are mostly invisible. Only data used in the fit are shown. b) Measured cross sections divided by predictions based on HERAPDF2.0Jets NNLO.

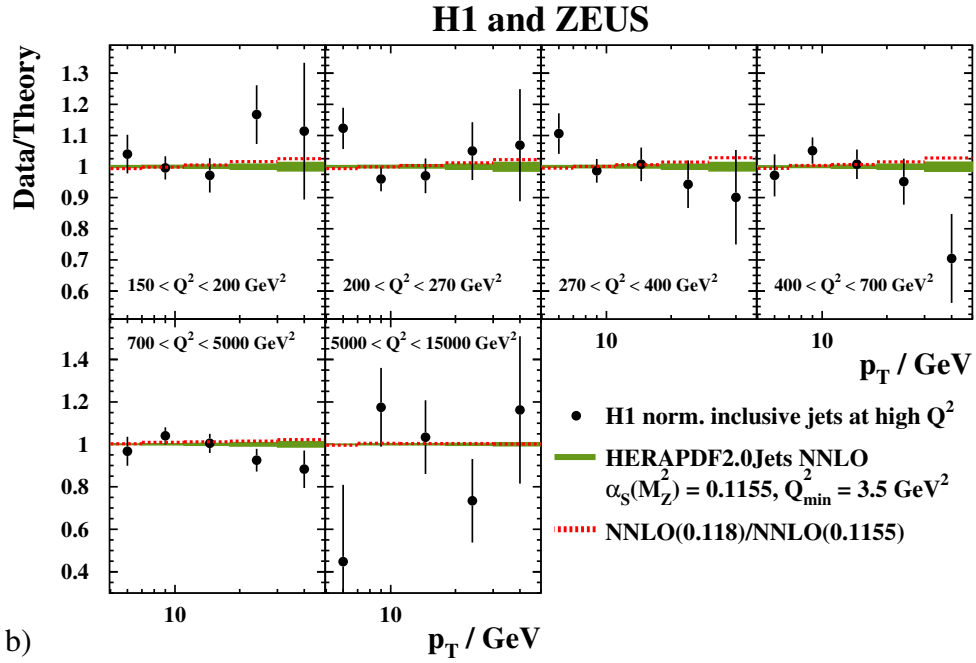
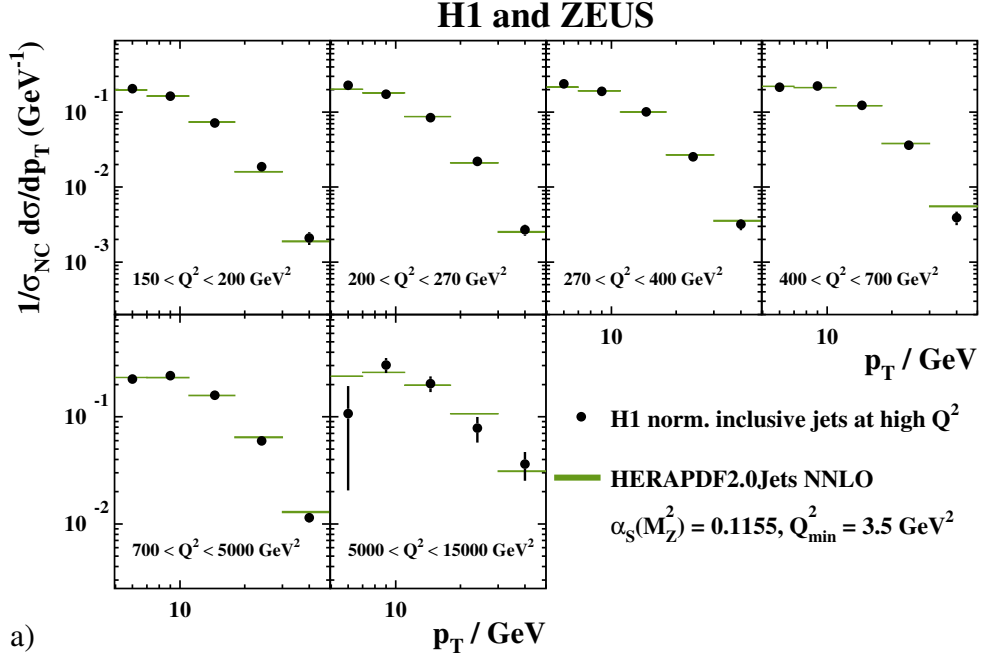


Figure 16: a) Differential inclusive jet cross sections, $d\sigma/dp_T$, normalised to NC inclusive cross sections, in bins of Q^2 between 150 and 15000 GeV^2 as measured by H1. Also shown are predictions based on HERAPDF2.0Jets NNLO. The bands represent the total uncertainties on the predictions excluding scale uncertainties; the bands are mostly invisible. Only data used in the fit are shown. b) Measured cross sections divided by predictions based on HERAPDF2.0Jets NNLO.

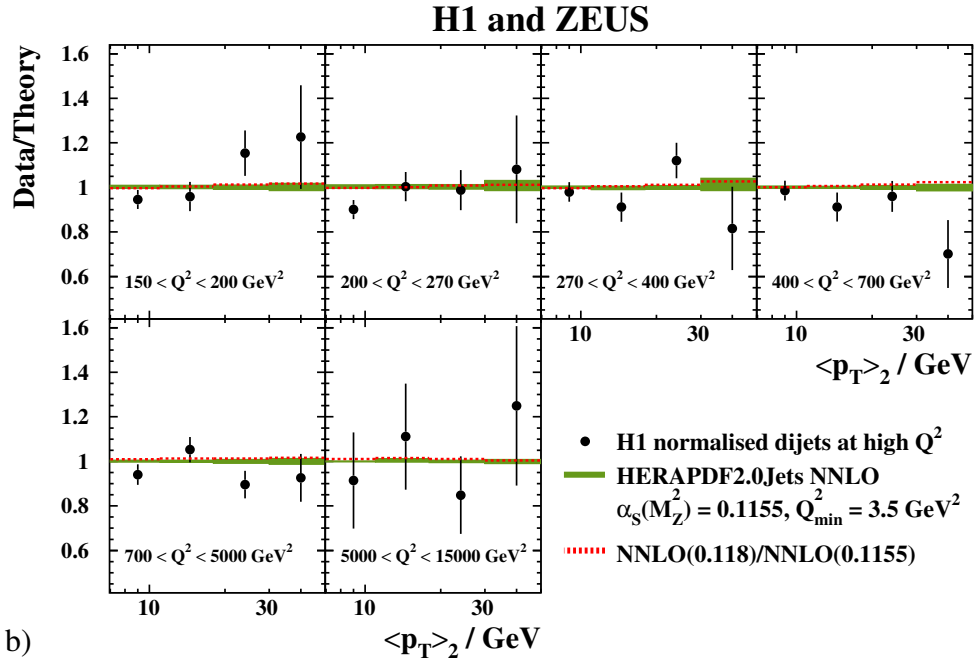
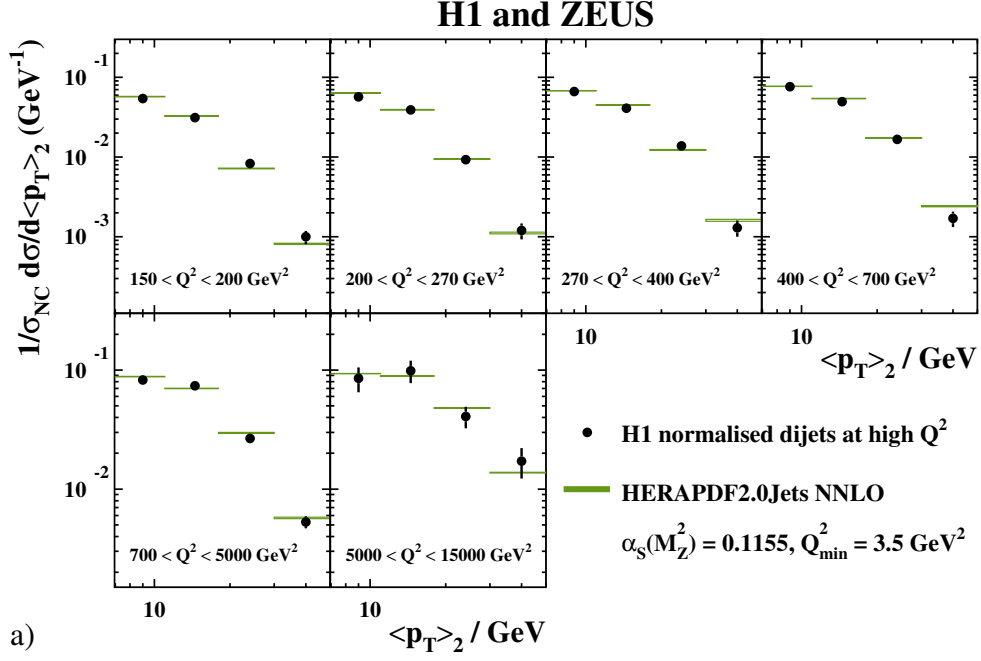


Figure 17: a) Differential dijet cross sections, $d\sigma/d\langle p_T \rangle_2$, normalised to NC inclusive cross sections, in bins of Q^2 between 150 and 15000 GeV^2 as measured by H1. The variable $\langle p_T \rangle_2$ denotes the average p_T of the two jets. Also shown are predictions based on HERAPDF2.0Jets NNLO. The bands represent the total uncertainties on the predictions excluding scale uncertainties; the bands are mostly invisible. Only data used in the fit are shown. b) Measured cross sections divided by predictions based on HERAPDF2.0Jets NNLO.

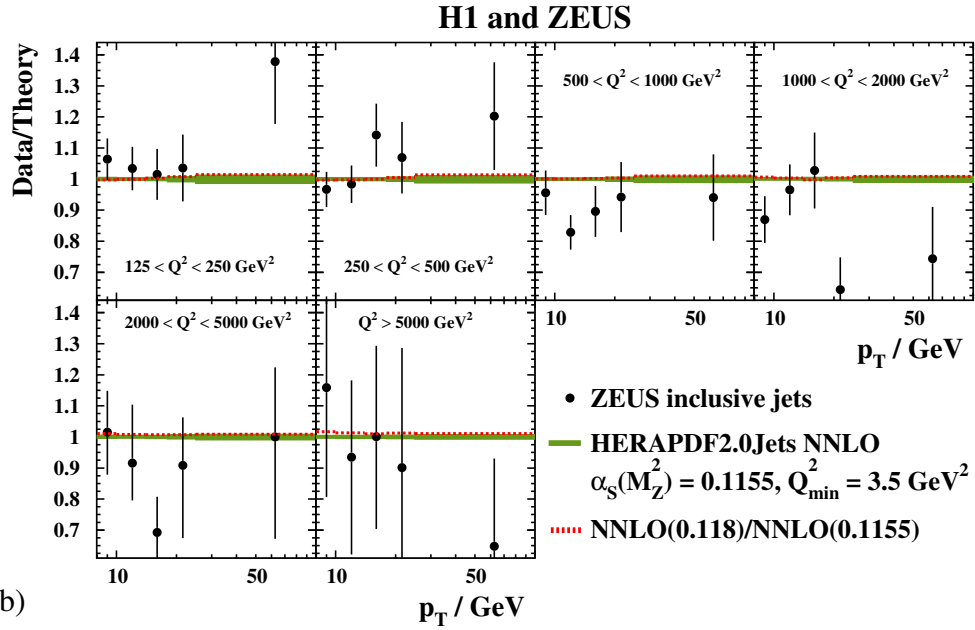
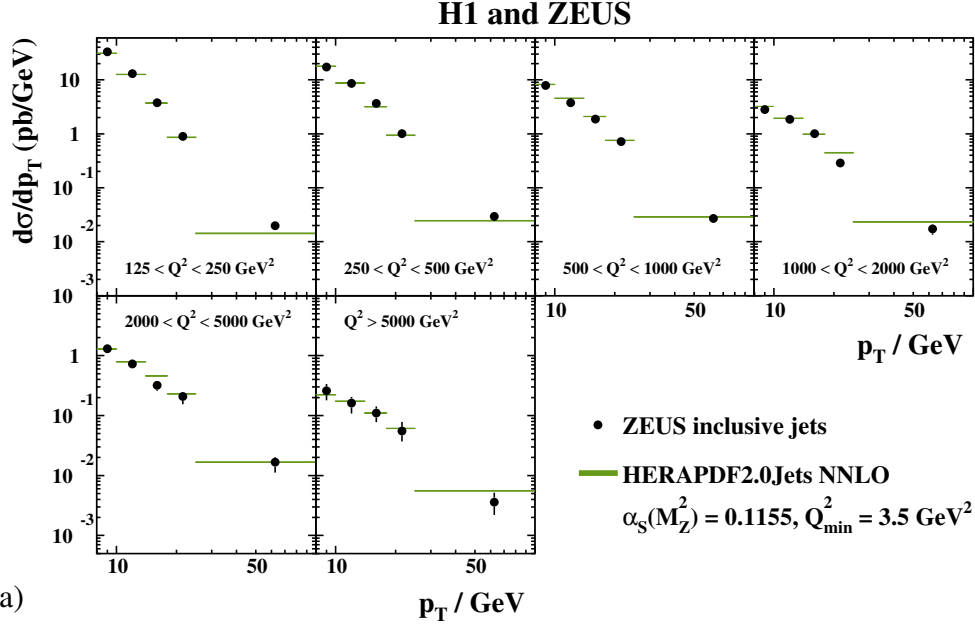


Figure 18: a) Differential jet cross sections, $d\sigma/dp_T$, in bins of Q^2 between 125 and 10000 GeV^2 as measured by ZEUS. Also shown are predictions based on HERAPDF2.0Jets NNLO. The bands represent the total uncertainty on the predictions excluding scale uncertainties; the bands are mostly invisible. Only data used in the fit are shown. b) Measured cross sections divided by predictions based on HERAPDF2.0Jets NNLO.

Appendix A:

PDF sets released

The following two sets of PDFs are released [41] and available on LHAPDF:
(<https://lhapdf.hepforge.org/pdfsets.html>).

- HERAPDF2.0Jets NNLO

- based on the combination of inclusive data from the H1 and ZEUS collaborations and selected data on jet production;
- with $Q_{\min}^2 = 3.5 \text{ GeV}^2$;
- using the RTOPT variable-flavour-number scheme;
 - * with fixed value of $\alpha_s(M_Z^2) = 0.01155$;
 - * with fixed value of $\alpha_s(M_Z^2) = 0.0118$;
- 14 eigenvector pairs give Hessian experimental (fit) uncertainties including hadronisation uncertainties;
- grids of 14 variations are released to describe the model and parameterisation uncertainties.

Appendix B:

Additional ratio plots on gluon PDF uncertainties

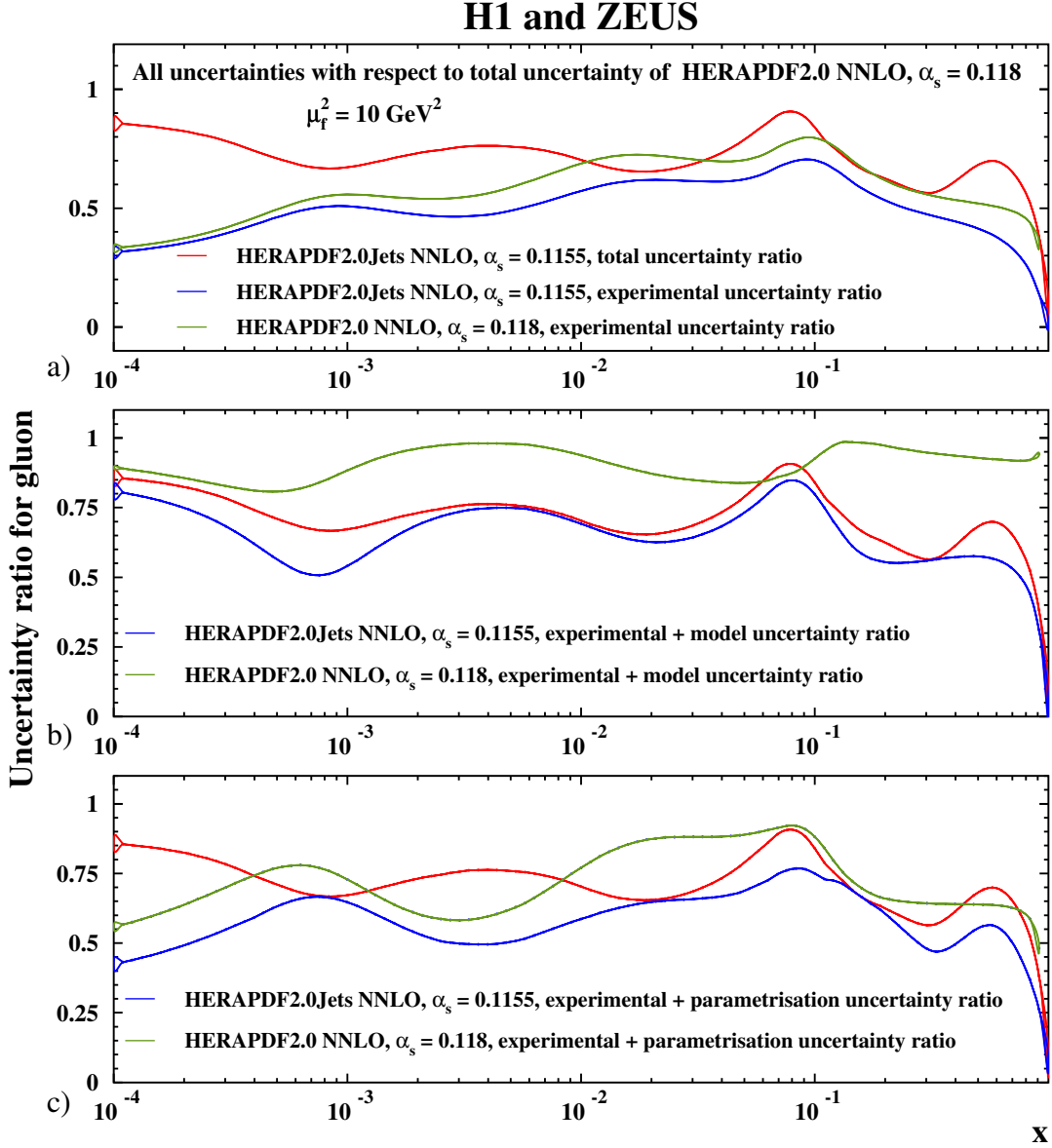


Figure 20: Ratios of uncertainties relative to the total uncertainties of HERAPDF2.0 NNLO $\alpha_s(M_Z^2) = 0.118$ for the total uncertainty of HERAPDF2.0Jets NNLO $\alpha_s(M_Z^2) = 0.1155$ and the a) experimental uncertainty of HERAPDF2.0Jets NNLO $\alpha_s(M_Z^2) = 0.1155$ as well as the experimental uncertainty of HERAPDF2.0 NNLO $\alpha_s(M_Z^2) = 0.118$, b) experimental plus model uncertainty of HERAPDF2.0Jets NNLO $\alpha_s(M_Z^2) = 0.1155$ as well as the experimental plus model uncertainty of HERAPDF2.0 NNLO $\alpha_s(M_Z^2) = 0.118$, c) experimental plus parameterisation uncertainty of HERAPDF2.0Jets NNLO $\alpha_s(M_Z^2) = 0.1155$ as well as the experimental plus parameterisation uncertainty of HERAPDF2.0 NNLO $\alpha_s(M_Z^2) = 0.118$, at the scale $\mu_f^2 = 10 \text{ GeV}^2$.

H1 and ZEUS

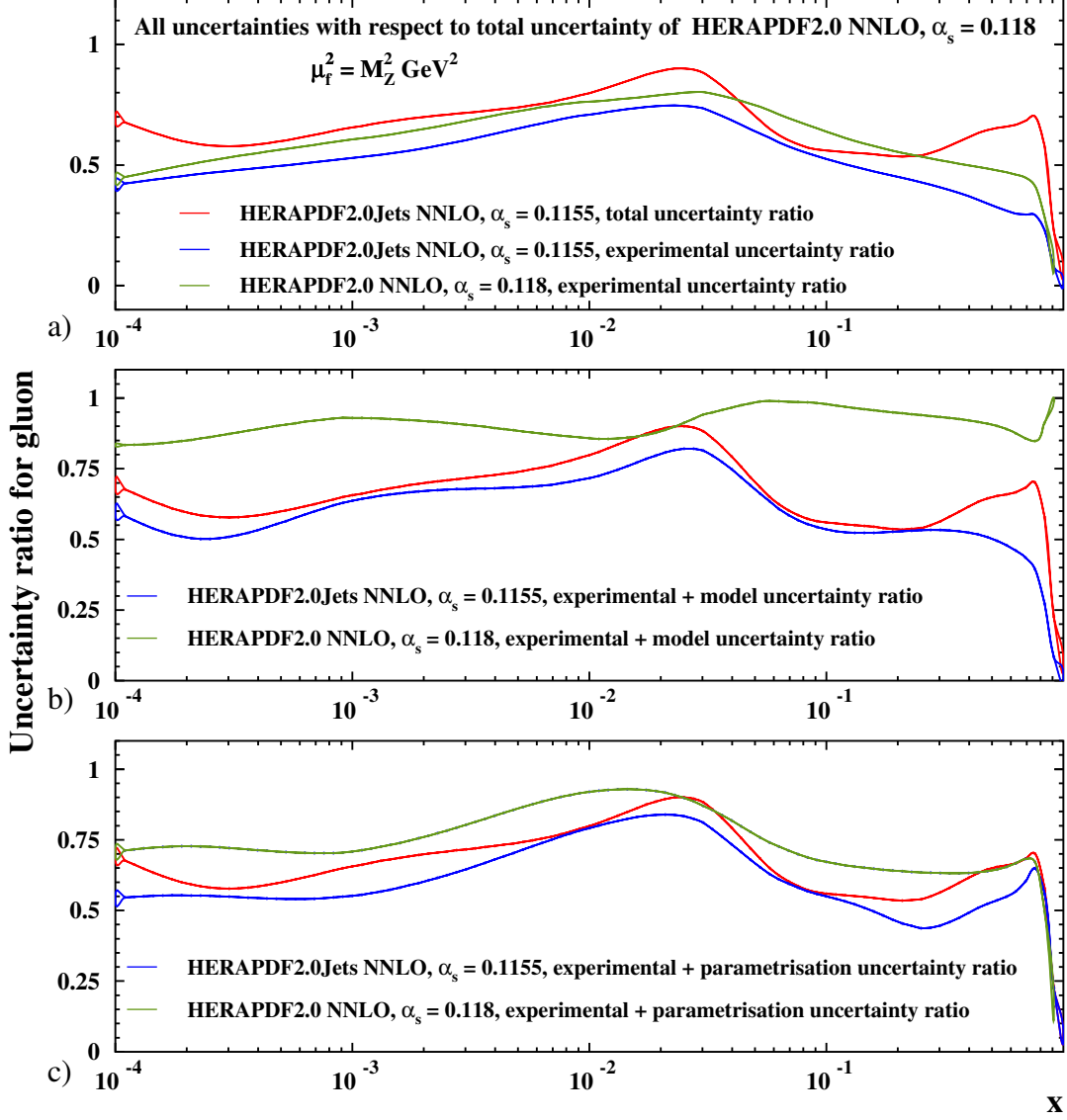


Figure 21: Ratios of uncertainties relative to the total uncertainties of HERAPDF2.0 NNLO $\alpha_s(M_Z^2) = 0.118$ for the total uncertainty of HERAPDF2.0Jets NNLO $\alpha_s(M_Z^2) = 0.1155$ and the a) experimental uncertainty of HERAPDF2.0Jets NNLO $\alpha_s(M_Z^2) = 0.1155$ as well as the experimental uncertainty of HERAPDF2.0 NNLO $\alpha_s(M_Z^2) = 0.118$, b) experimental plus model uncertainty of HERAPDF2.0Jets NNLO $\alpha_s(M_Z^2) = 0.1155$ as well as the experimental plus model uncertainty of HERAPDF2.0 NNLO $\alpha_s(M_Z^2) = 0.118$, c) experimental plus parameterisation uncertainty of HERAPDF2.0Jets NNLO $\alpha_s(M_Z^2) = 0.1155$ as well as the experimental plus parameterisation uncertainty of HERAPDF2.0 NNLO $\alpha_s(M_Z^2) = 0.118$, at the scale $\mu_f^2 = M_Z^2$.

H1 and ZEUS

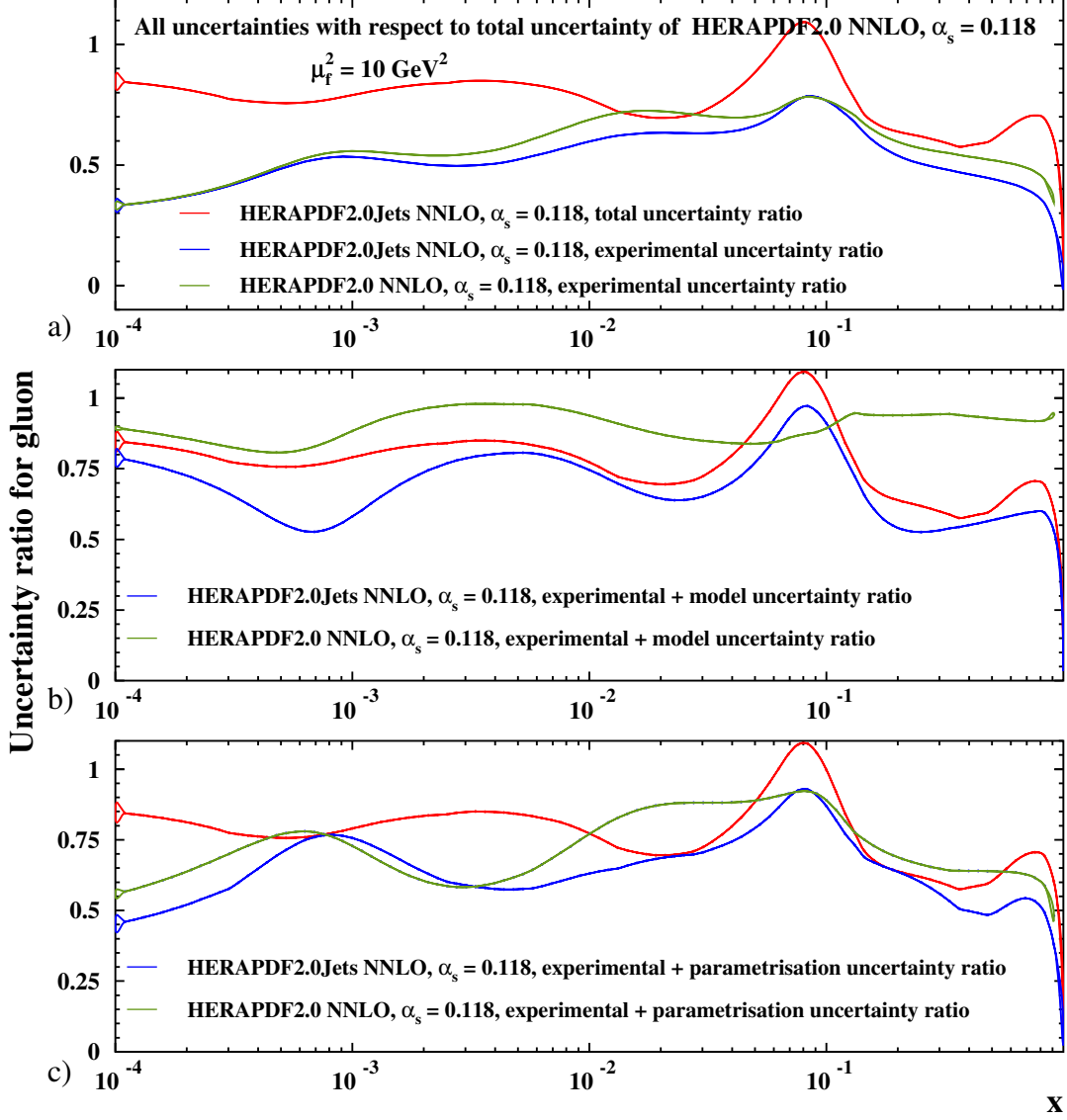


Figure 22: Ratios of uncertainties relative to the total uncertainties of HERAPDF2.0 NNLO $\alpha_s(M_Z^2) = 0.118$ for the total uncertainty of HERAPDF2.0Jets NNLO $\alpha_s(M_Z^2) = 0.118$ and the a) experimental uncertainty of HERAPDF2.0Jets NNLO $\alpha_s(M_Z^2) = 0.118$ as well as the experimental uncertainty of HERAPDF2.0 NNLO $\alpha_s(M_Z^2) = 0.118$, b) experimental plus model uncertainty of HERAPDF2.0Jets NNLO $\alpha_s(M_Z^2) = 0.118$ as well as the experimental plus model uncertainty of HERAPDF2.0 NNLO $\alpha_s(M_Z^2) = 0.118$, c) experimental plus parameterisation uncertainty of HERAPDF2.0Jets NNLO $\alpha_s(M_Z^2) = 0.118$ as well as the experimental plus parameterisation uncertainty of HERAPDF2.0 NNLO $\alpha_s(M_Z^2) = 0.118$, at the scale $\mu_f^2 = 10 \text{ GeV}^2$.

H1 and ZEUS

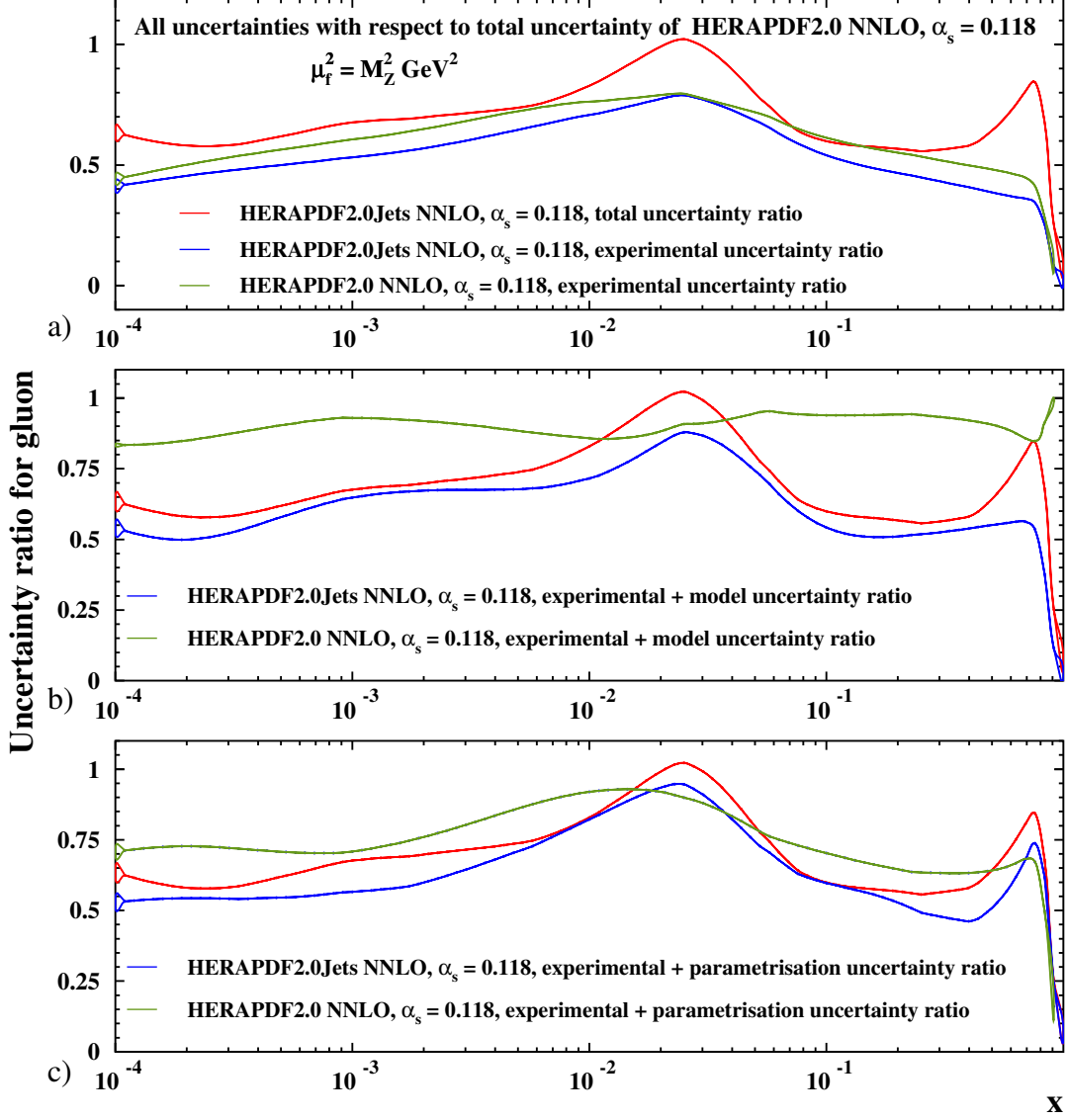


Figure 23: Ratios of uncertainties relative to the total uncertainties of HERAPDF2.0 NNLO $\alpha_s(M_Z^2) = 0.118$ for the total uncertainty of HERAPDF2.0Jets NNLO $\alpha_s(M_Z^2) = 0.118$ and the a) experimental uncertainty of HERAPDF2.0Jets NNLO $\alpha_s(M_Z^2) = 0.118$ as well as the experimental uncertainty of HERAPDF2.0 NNLO $\alpha_s(M_Z^2) = 0.118$, b) experimental plus model uncertainty of HERAPDF2.0Jets NNLO $\alpha_s(M_Z^2) = 0.118$ as well as the experimental plus model uncertainty of HERAPDF2.0 NNLO $\alpha_s(M_Z^2) = 0.118$, c) experimental plus parameterisation uncertainty of HERAPDF2.0Jets NNLO $\alpha_s(M_Z^2) = 0.118$ as well as the experimental plus parameterisation uncertainty of HERAPDF2.0 NNLO $\alpha_s(M_Z^2) = 0.118$, at the scale $\mu_f^2 = M_Z^2$.

Internal extra material:⁷

Comparison of results on $\alpha_s(M_Z^2)$ determined at NLO and NNLO:

A more detailed comparison between the NLO and NNLO results must account for the following differences:

- the choice of scale was different;
- the NLO result did not include the recently published H1 low- Q^2 inclusive and dijet data [13];
- the NLO result did not include the newly published low p_T points from the H1 high- Q^2 inclusive data;
- the NNLO result does not include trijet data;
- the NNLO result does not include the low p_T points from the ZEUS dijet data;
- the NNLO analysis imposes a stronger kinematic cut $\mu > 13.5$ GeV;
- the treatment of hadronisation uncertainty differs.

All these changes with respect to the NLO analysis had to be made to create a consistent environment for a fit at NNLO. At the same time, an NLO fit cannot be done under exactly the same conditions as the NNLO fit since the H1 low Q^2 data cannot be well fitted at NLO. However, an NLO and an NNLO fit can be done under the common conditions:

- choice of scale, $\mu_f^2 = \mu_r^2 = Q^2 + p_T^2$;
- exclusion of the H1 low- Q^2 inclusive and dijet data;
- exclusion of the low- p_T points from the H1 high- Q^2 inclusive jet data;
- exclusion of trijet data;
- exclusion of low- p_T points from the ZEUS dijet data;
- exclusion of data with $\mu < 13.5$ GeV;
- hadronisation uncertainties treated as correlated systematic uncertainties as done in the NNLO analysis.

In this case, the values obtained were $\alpha_s(M_Z^2) = 0.1186 \pm 0.0014(\text{exp})$ at NLO and $\alpha_s(M_Z^2) = 0.1144 \pm 0.0013(\text{exp})$ at NNLO. The new NLO value of $\alpha_s(M_Z^2)$ agrees with the published [2] value of 0.1183. The change of the NNLO result from the preferred value of 0.1156 is mostly due to the exclusion of the H1 low Q^2 data and the low- p_T points at high Q^2 .

⁷This material was Appendix A and was moved to internal extra material according to an EB decision.

Internal extra material:⁸

More detailed information concerning the source of uncertainties at a scale of 10 GeV^2 : The green band represents HERAPDF2.0Jets NNLO $\alpha_s(M_Z^2)=0.1155$ as obtained for the old procedure, i.e. with double counting.

This shows that the improvement is mainly due to jet data.

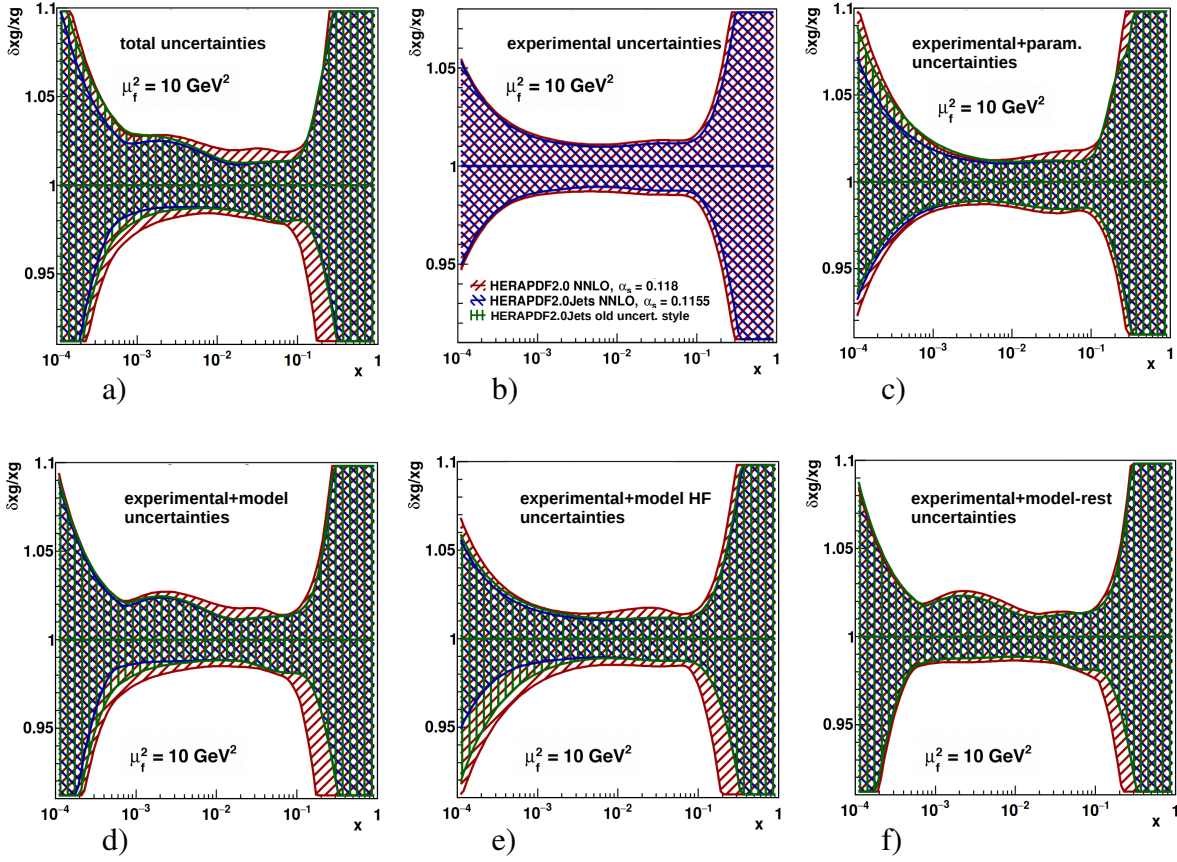


Figure 24: Comparison of the normalised uncertainties on the gluon PDFs of HERAPDF2.0Jets NNLO, HERAPDF2.0 NNLO and HERAPDF2.0Jets NNLO with old procedure on uncertainties for a) total, b) experimental, i.e. fit, c) experimental plus parameterisation, d) experimental plus model, e) experimental plus model due to heavy flavour f) experimental plus all model but heavy flavour uncertainties at the scale $\mu_f^2 = 10 \text{ GeV}^2$. The uncertainties on the three gluon distributions are shown as differently hatched bands.

⁸This material was public extra material and was moved to internal extra material according to an EB decision.

Internal extra material:⁹

More detailed information concerning the source of uncertainties at a scale of M_W^2 : The green band represents HERAPDF2.0Jets NNLO $\alpha_s(M_Z^2)=0.1155$ as obtained for the old procedure, i.e. with double counting.

This shows that the improvement is mainly due to jet data.

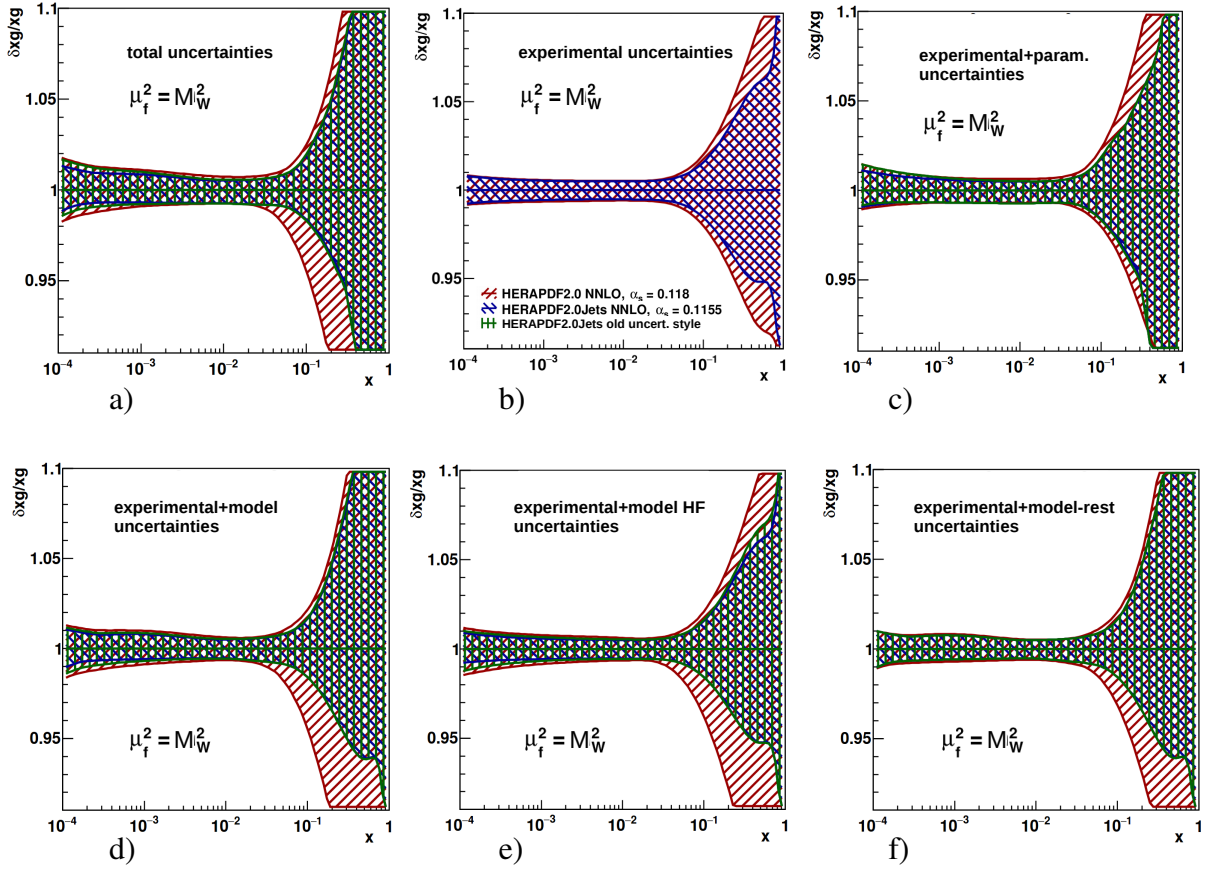


Figure 25: Comparison of the normalised uncertainties on the gluon PDFs of HERAPDF2.0Jets NNLO, HERAPDF2.0 NNLO and HERAPDF2.0Jets NNLO with old procedure on uncertainties for a) total, b) experimental, i.e. fit, c) experimental plus parameterisation, d) experimental plus model, e) experimental plus model due to heavy flavour f) experimental plus all model but heavy flavour uncertainties at the scale $\mu_f^2 = M_W^2$. The uncertainties on the three gluon distributions are shown as differently hatched bands.

⁹This material was external extra material and was moved to internal extra material according to an EB decision.

Internal extra material: ¹⁰

```
507
508
509 Parameters as determined by the fits and their correlations
510 =====
511
512 PARAMETERS WITH UNCERTAINTIES:
513 =====
514 as free
515 =====
516
517 2 'Bg' -0.084608 0.071758
518 3 'Cg' 6.145485 0.553362
519 7 'Aprig' 0.148366 0.134036
520 8 'Bprig' -0.408486 0.062832
521 9 'Cprig' 25.000000 0.000000 fixed
522 12 'Buv' 0.782478 0.027706
523 13 'Cuv' 4.878155 0.083909
524 15 'Euv' 10.390885 1.352200
525 22 'Bdv' 0.983110 0.083080
526 23 'Cdv' 4.795152 0.383854
527 33 'CUbar' 7.123114 1.699099
528 34 'DUbar' 1.995344 2.431042
529 41 'ADbar' 0.262598 0.010781
530 42 'BDbar' -0.128810 0.004899
531 43 'CDbar' 9.094971 1.741850
532 101 'alphas' 0.115638 0.001142
533
534 as = 0.1155
535 =====
536
537 2 'Bg' -0.085574 0.039648
538 3 'Cg' 6.171545 0.496131
539 7 'Aprig' 0.147903 0.040820
540 8 'Bprig' -0.409380 0.028287
541 9 'Cprig' 25.000000 0.000000 fixed
542 12 'Buv' 0.781078 0.025867
543 13 'Cuv' 4.880050 0.080411
544 15 'Euv' 10.401539 1.289019
545 22 'Bdv' 0.983055 0.084572
546 23 'Cdv' 4.804735 0.380423
547 33 'CUbar' 7.125150 1.645404
548 34 'DUbar' 2.031948 2.222251
549 41 'ADbar' 0.262191 0.010036
550 42 'BDbar' -0.128934 0.004725
551 43 'CDbar' 9.161993 1.693978
552
553 as = 0.118
554 =====
555
556 2 'Bg' -0.070319 0.043016
557 3 'Cg' 5.670899 0.482567
558 7 'Aprig' 0.161572 0.043068
559 8 'Bprig' -0.391610 0.027755
560 9 'Cprig' 25.000000 0.000000 fixed
561 12 'Buv' 0.806334 0.028281
562 13 'Cuv' 4.844608 0.081284
563 15 'Euv' 10.242348 1.441602
564 22 'Bdv' 0.981522 0.092135
565 23 'Cdv' 4.622768 0.397334
566 33 'CUbar' 7.137838 1.347568
567 34 'DUbar' 1.458837 1.614989
568 41 'ADbar' 0.269978 0.010673
569 42 'BDbar' -0.126504 0.004831
570 43 'CDbar' 8.036277 1.509073
571
572
573
574
575 PARAMETER CORRELATION COEFFICIENTS
576 =====
577 as free
578 =====
579
580 NO. GLOBAL 2 3 7 8 12 13 15 22 23 33 34 41 42 43 101
581 2 0.99909 1.000 0.544-0.880-0.627 0.112-0.024-0.040 0.030-0.015 0.024 0.019-0.090-0.166-0.066 0.135
582 3 0.99544 0.544 1.000-0.294-0.077-0.034 0.078-0.036-0.095-0.060 0.141 0.242-0.452-0.503-0.226-0.386
583 7 0.99942 -0.880-0.294 1.000 0.914 0.101-0.067-0.115 0.033 0.028 0.010-0.001 0.025 0.028-0.026 0.002
584 8 0.99710 -0.627-0.077 0.914 1.000 0.251-0.130-0.230 0.094 0.057 0.010-0.028 0.038-0.009-0.062 0.093
585 12 0.99580 0.112-0.034 0.101 0.251 1.000-0.208-0.711 0.254 0.050 0.326 0.036 0.524 0.400 0.021 0.418
586 13 0.98055 -0.024 0.078-0.067-0.130-0.208 1.000 0.708-0.193-0.212 0.374 0.410-0.168-0.124-0.089-0.183
587 15 0.99428 -0.040-0.036-0.115-0.230-0.711 0.708 1.000-0.226-0.165 0.133 0.338-0.369-0.299-0.137-0.056
588 22 0.99034 0.030-0.095 0.033 0.094 0.254-0.193-0.226 1.000 0.892 0.370 0.287 0.266 0.228 0.591 0.020
589 23 0.98232 -0.015-0.060 0.028 0.057 0.050-0.212-0.165 0.892 1.000 0.151 0.114 0.154 0.147 0.553-0.197
590 33 0.99829 0.024 0.141 0.010 0.010 0.326 0.374 0.133 0.370 0.151 1.000 0.923-0.006-0.020 0.160 0.002
591 34 0.99812 0.019 0.242-0.001-0.028 0.036 0.410 0.338 0.287 0.114 0.923 1.000-0.253-0.252 0.228-0.108
592 41 0.97212 -0.090-0.452 0.025 0.038 0.524-0.168-0.369 0.266 0.154-0.006-0.253 1.000 0.950 0.168 0.330
593 42 0.97595 -0.166-0.503 0.028-0.009 0.400-0.124-0.299 0.228 0.147-0.020-0.252 0.950 1.000 0.188 0.220
594 43 0.98859 -0.066-0.226-0.026-0.062 0.021-0.089-0.137 0.591 0.553 0.160 0.228 0.168 0.188 1.000-0.291
595 101 0.99603 0.135-0.386 0.002 0.093 0.418-0.183-0.056 0.020-0.197 0.002-0.108 0.330 0.220-0.291 1.000
596
```

¹⁰The EB decided to have the information on parameters and their correlations in an ascii file for internal usage.

```

597 as = 0.1155
598 =====
599
600 NO. GLOBAL 2 3 7 8 12 13 15 22 23 33 34 41 42 43
601 2 0.99909 1.000 0.653-0.891-0.656 0.060 0.002-0.031 0.027 0.012 0.023 0.033-0.145-0.204-0.027
602 3 0.99467 0.653 1.000-0.325-0.056 0.160 0.023-0.053-0.078-0.144 0.171 0.230-0.374-0.465-0.372
603 7 0.99943 -0.891-0.325 1.000 0.920 0.109-0.063-0.112 0.034 0.029 0.014 0.004 0.028 0.032-0.025
604 8 0.99712 -0.656-0.056 0.920 1.000 0.231-0.111-0.221 0.092 0.076 0.012-0.013 0.010-0.027-0.035
605 12 0.99499 0.060 0.160 0.109 0.231 1.000-0.117-0.734 0.285 0.154 0.379 0.134 0.442 0.340 0.171
606 13 0.98052 0.002 0.023-0.063-0.111-0.117 1.000 0.713-0.154-0.239 0.418 0.433-0.118-0.092-0.132
607 15 0.99429 -0.031-0.053-0.112-0.221-0.734 0.713 1.000-0.203-0.171 0.161 0.344-0.373-0.296-0.148
608 22 0.99053 0.027-0.078 0.034 0.092 0.285-0.154-0.203 1.000 0.910 0.404 0.331 0.265 0.220 0.625
609 23 0.98154 0.012-0.144 0.029 0.076 0.154-0.239-0.171 0.910 1.000 0.169 0.115 0.233 0.196 0.530
610 33 0.99858 0.023 0.171 0.014 0.012 0.379 0.418 0.161 0.404 0.169 1.000 0.940-0.017-0.033 0.192
611 34 0.99841 0.033 0.230 0.004-0.013 0.134 0.433 0.344 0.331 0.115 0.940 1.000-0.223-0.229 0.228
612 41 0.96869 -0.145-0.374 0.028 0.010 0.442-0.118-0.373 0.265 0.233-0.017-0.223 1.000 0.953 0.287
613 42 0.97473 -0.204-0.465 0.032-0.027 0.340-0.092-0.296 0.220 0.196-0.033-0.229 0.953 1.000 0.264
614 43 0.98749 -0.027-0.372-0.025-0.035 0.171-0.132-0.148 0.625 0.530 0.192 0.228 0.287 0.264 1.000
615
616 as = 0.118
617 =====
618
619 NO. GLOBAL 2 3 7 8 12 13 15 22 23 33 34 41 42 43
620 2 0.99830 1.000 0.584-0.794-0.507 0.052-0.002-0.029-0.005-0.017 0.025 0.045-0.188-0.238-0.067
621 3 0.99467 0.584 1.000-0.086 0.184 0.146-0.004-0.071-0.148-0.192 0.160 0.233-0.432-0.517-0.453
622 7 0.99906 -0.794-0.086 1.000 0.917 0.190-0.095-0.183 0.071 0.059 0.029 0.015-0.019-0.048-0.030
623 8 0.99645 -0.507 0.184 0.917 1.000 0.308-0.142-0.288 0.115 0.094 0.033 0.008-0.065-0.131-0.053
624 12 0.99521 0.052 0.146 0.190 0.308 1.000-0.176-0.777 0.302 0.184 0.381 0.166 0.429 0.321 0.216
625 13 0.98045 -0.002-0.004-0.095-0.142-0.176 1.000 0.712-0.219-0.278 0.360 0.389-0.112-0.079-0.150
626 15 0.99461 -0.029-0.071-0.183-0.288-0.777 0.712 1.000-0.258-0.208 0.089 0.264-0.354-0.270-0.188
627 22 0.99185 -0.005-0.148 0.071 0.115 0.302-0.219-0.258 1.000 0.920 0.351 0.291 0.287 0.238 0.666
628 23 0.98399 -0.017-0.192 0.059 0.094 0.184-0.278-0.208 0.920 1.000 0.159 0.107 0.248 0.208 0.556
629 33 0.99867 0.025 0.160 0.029 0.033 0.381 0.360 0.089 0.351 0.159 1.000 0.948 0.010-0.006 0.135
630 34 0.99849 0.045 0.233 0.015 0.008 0.166 0.389 0.264 0.291 0.107 0.948 1.000-0.178-0.186 0.157
631 41 0.96829 -0.188-0.432-0.019-0.065 0.429-0.112-0.354 0.287 0.248 0.010-0.178 1.000 0.953 0.337
632 42 0.97500 -0.238-0.517-0.048-0.131 0.321-0.079-0.270 0.238 0.208-0.006-0.186 0.953 1.000 0.312
633 43 0.99021 -0.067-0.453-0.030-0.053 0.216-0.150-0.188 0.666 0.556 0.135 0.157 0.337 0.312 1.000
634
635

```